N-ADAMANTYL-ANTHRANIL AMIDE DERIVATIVES: NEW SELECTIVE LIGANDS FOR THE CANNABINOID RECEPTOR SUBTYPE 2 (CB2R)

*Giovanni Graziano,[a#] Pietro Delre,[b#] Francesca Carofiglio,[a] Jose Brea,[c,d] Alessia Ligresti,[e] Magdalena Kostrzewa,[e] Chiara Riganti,[f] Claudia Gioè-Gallo,[g] Maria Majellaro,[g] Orazio Nicolotti,[a] Nicola Antonio Colabufo,[a] Carmen Abate,[a,b] Maria Isabel Loza,[c,d] Eddy Sotelo,[g] Giuseppe Felice Mangiatordi,[b] Marialessandra Contino,[*a] Angela Stefanachi[*a] and Francesco Leonetti.[a]*

[a] Department of Pharmacy-Pharmaceutical Sciences, University of the Studies of Bari "Aldo Moro", via E.Orabona 4, 70125-Bari, Italy

[b] CNR – Institute of Crystallography, Via Giovanni Amendola, 122/O, 70126-Bari, Italy

[c] Center for Research in Molecular Medicine and Chronic Diseases (CIMUS), University of Santiago de Compostela, Av. Barcelona, 15782-Santiago de Compostela, Spain

[d] Department of Pharmacology, Pharmacy and Pharmaceutical Technology. School of Pharmacy. University of Santiago de Compostela, Santiago de Compostela, Spain

[e] Institute of Biomolecular Chemistry, National Research Council of Italy, Via Campi Flegrei 34, 80078 Pozzuoli (Na), Italy;

[f] Department of Oncology, University of Turin, Turin, Italy.

[g]Centro Singular de Investigación en Química Biolóxica e Materiais Moleculares (CiQUS) and Departamento de Química Orgánica, Universidade de Santiago de Compostela, Santiago de Compostela 15782, Spain.

# These two authors contributed equally to the manuscript

KEYWORDS

CB2R, anti-inflammatory, immune-modulatory, *N*-adamantyl-anthranil amide derivatives, CB2R agonism and CB2R antagonism.

ABSTRACT

Cannabinoid type 2 receptor (CB2R) is a G-protein-coupled receptor that, together with Cannabinoid type 1 receptor (CB1R), endogenous cannabinoids and enzymes responsible for their synthesis and degradation, forms the EndoCannabinoid System (ECS). In the last decade, several studies have shown that CB2R is overexpressed in activated central nervous system (CNS) microglia cells, in disorders based on an inflammatory state, such as neurodegenerative diseases, neuropathic pain, and cancer. For this reason, the anti-inflammatory and immune-modulatory potentials of CB2R ligands are emerging as a novel therapeutic approach. The design of selective ligands is however hampered by the high sequence homology of transmembrane domains of CB1R and CB2R. Based on a recent three-arm pharmacophore hypothesis and latest CB2R crystal structures, we designed, synthesized, and evaluated a series of new *N*-adamantyl-anthranil amide derivatives as CB2R selective ligands. Interestingly, this new class of compounds displayed a high affinity for human CB2R along with an excellent selectivity respect to CB1R. In this respect, compounds exhibiting the best pharmacodynamic profile in terms of CB2R affinity were also evaluated for the functional behavior and molecular docking simulations provided a sound rationale by highlighting the relevance of the arm 1 substitution to prompt CB2R action. Moreover, the modulation of the pro- and anti-inflammatory cytokines production was also investigated to exert the ability of the best compounds to modulate the inflammatory cascade.

INTRODUCTION

The endocannabinoid system (ECS) is a highly conserved lipid signaling network in all vertebrates, including humans. It is involved in the homeostatic control of several physiological functions, and is the focus of considerable research efforts aimed at its therapeutic exploitation.[1–3] ECS consists of: i) two types of G-protein-coupled receptors,[4] mainly differing for their tissue expression pattern[5,6] and ii) endogenous cannabinoids and enzymes responsible for their synthesis and degradation. So far, two major cannabinoid-specific receptors, named Cannabinoid receptor subtype 1 (CB1R)[7] and Cannabinoid receptor subtype 2 (CB2R), have been cloned and characterized from mammalian tissues.[8,9] In addition, other receptors, including the transient receptor potential cation channel subfamily V member 1 (TRPV1) and certain orphan G protein-coupled receptors (GPR55, GPR119, and GPR18) have been proposed to act as endocannabinoid receptors and defined as non-canonical cannabinoid receptors.[8,10] ECS is also composed of: i) endogenous agonists for these receptors that are known as 'endocannabinoids' and include anandamide and 2-arachidonoyl glycerol; and ii) enzymes responsible for endocannabinoid biosynthesis, cellular uptake and degradative metabolism.[11–13] CB1R is expressed throughout the body and it is abundantly distributed in the central nervous system (CNS);[14,15] it mediates the psychotropic effects of Δ^9-tetrahydrocannabinol (Δ^9-THC).[16,17] CB1R has been also localized in extracerebral tissues such as the gastrointestinal tract, adipose tissue, liver, uterus, and prostate.[18–21] CB2R has been, instead, essentially found in cells and tissues associated with the immune system,[8,22,23] although very low concentrations have been also found in the brain,[24–26] gastrointestinal tract tissues and other cells such as vascular endothelial cells, cardiomyocytes, and bone cells.[27] In the last few years, CB2R modulation has disclosed many potential therapeutic effects[8,13,28] since overexpression of the receptor has been detected in activated microglia and infiltrated macrophages in the brain,[22,29–31] in disorders based on an inflammatory state such as neurodegenerative diseases,[29,32–39] in acute pain, persistent inflammatory pain, postoperative pain, cancer pain and neuropathic pain[11,40–44] and in cancer cells.[25,45–50]

At the CNS level, CB2R activation leads to microglia polarization from the M1-state (the microglia pro-inflammatory phenotype, characterized by pro-inflammatory cytokines production) to the M2-state (the microglia anti-inflammatory phenotype, characterized by anti-inflammatory cytokines production). This anti-inflammatory effect has been hypothesized as a therapeutic strategy to block the persistent inflammation (neuroinflammation) in neurodegenerative diseases, but also to block the "cytokines storm" proper of Coronavirus Disease 19 (COVID-19)and also the persistent inflammatory state found in the onset of several types of tumours (ref).

P~~In addition, p~~reclinical studies have demonstrated the critical role of CB2R in the inflammatory process associated with rheumatoid arthritis, inflammatory bowel diseases, atherosclerosis or liver ischemia-reperfusion injury.[51–56] For this reason, the anti-inflammatory, and the immune-modulatory actions of CB2R agonists have potential roles for treating these diseases.[28,57–61] Moreover, given the involvement of CB2R ~~receptors~~ in immunomodulatory processes, the possible role of the CB2R ~~receptor~~ in the modulation of the inflammatory and cytokines misbalance, observed in ~~Coronavirus Disease 19 (~~COVID-19~~)~~ patients, was also proposed.[62]

CB2R antagonists have been less investigated[63] but recent studies indicate that CB2R antagonists can ameliorate renal fibrosis[64] and delay tumor progression,[65] indicating their potential as compounds for treating fibrotic conditions and cancer. However, there are many pieces of evidence that CB2R antagonists may be a good therapeutic option in the treatment of inflammation associated with obesity, insulin resistance, and non-alcoholic fatty liver disease (NAFLD).[66]

In the last years, interesting papers presented the design and the synthesis of new CB2R antagonist[67,68] suggesting that additional studies aimed at characterizing the pharmacophore portion responsible for activation at functional level are becoming essential in the field.

In this study, we aimed to discover new selective CB2R ligands as promising drugs devoid of the psychotropic side effects, associated with drugs abuse due to the CB1R interference.[69,70]

CB2R has a high degree of homology with CB1R, sharing 44% of sequence identity and 68% of sequence similarity in the transmembrane region, which contains the binding site, thus complicating

Commentato [ac1]: ***Cannabinoid Receptor Subtype 2 (CB2R) in a Multitarget Approach: Perspective of an Innovative Strategy in Cancer and Neurodegeneration | Journal of Medicinal Chemistry*. https://pubs.acs.org/doi/pdf/10.1021/acs.jmedchem.0c01357 (accessed 2022-06-06).**
(7) Zhang, J.; Zhang, S.; Liu, Y.; Su, M.; Ling, X.; Liu, F.; Ge, Y.; Bai, M. Combined CB2 Receptor Agonist and Photodynamic Therapy Synergistically Inhibit Tumor Growth in Triple Negative Breast Cancer. *Photodiagnosis Photodyn Ther* 2018, *24*, 185–191. https://doi.org/10.1016/j.pdpdt.2018.09.006.
(8) Kisková, T.; Mungenast, F.; Suváková, M.; Jäger, W.; Thalhammer, T. Future Aspects for Cannabinoids in Breast Cancer Therapy. *Int J Mol Sci* 2019, *20* (7), 1673. https://doi.org/10.3390/ijms20071673.
(9) Morales, P.; Jagerovic, N. Antitumor Cannabinoid Chemotypes: Structural Insights. *Front Pharmacol* 2019, *10*, 621. https://doi.org/10.3389/fphar.2019.00621.
(10) Rastegar, M.; Samadizadeh, S.; Yasaghi, M.; Moradi, A.; Tabarraei, A.; Salimi, V.; Tahamtan, A. Functional Variation (Q63R) in the Cannabinoid CB2 Receptor May Affect the Severity of COVID-19: A Human Study and Molecular Docking. *Arch Virol* 2021, *166* (11), 3117–3126. https://doi.org/10.1007/s00705-021-05223-7.
(11) Rb, van B.; Rn, M.; Ta, B.; Jb, W.; Hc, L.; S, F.; Fg, T. Cannabinoids Block Cellular Entry of SARS-CoV-2 and the Emerging Variants. *Journal of natural products* 2022, *85* (1). https://doi.org/10.1021/acs.jnatprod.1c00946.
(12) Nagoor Meeran, M. F.; Sharma, C.; Goyal, S. N.; Kumar, S.; Ojha, S. CB2 Receptor-selective Agonists as Candidates for Targeting Infection, Inflammation, and Immunity in SARS-CoV-2 Infections. *Drug Dev Res* 2020, 10.1002/ddr.21752. https://doi.org/10.1002/ddr.21752.
(13) *Frontiers | β-Caryophyllene, A Natural Dietary CB2 Receptor Selective Cannabinoid can be a Candidate to Target the Trinity of Infection, Immunity, and Inflammation in COVID-19 | Pharmacology*. https://www.frontiersin.org/articles/10.3389/fphar.2021.590201/full (accessed 2022-06-06).
(14) Rossi, F.; Tortora, C.; Argenziano, M.; Di Paola, A.; Punzo, F. Cannabinoid Receptor Type 2: A Possible Target in SARS-CoV-2 (CoV-19) Infection? *Int J Mol Sci* 2020, *21* (11), 3809. https://doi.org/10.3390/ijms21113809.

Formattato: Evidenziato

Formattato: Evidenziato

Formattato: Evidenziato

97 the development of selective CBR ligands.[9] In fact, many CB2R ligands also modulate CB1R, making
98 the understanding of the individual signaling contributions difficult. However, the recent release of
99 two CB2R crystal structures, one complexed with an agonist and the other with an antagonist,[4,71]
100 represents an unprecedented opportunity to guide at a molecular level of detail the rational discovery
101 of newer and selective ligands. In this respect, we focused on the design and synthesis of CB2R
102 selective ligands based for the first time on the *N*-adamantyl-anthranil amide scaffold (Figure 1 B).
103 The first important contribution for the rational design of CB2R selective ligands was given by Zhi-
104 Jie Liu and co-workers, who solved, for the first time, a CB2R crystal structure (resolution 2.8 Å).[71]
105 Importantly, the protein was crystallized in complex with the synthetic antagonist AM10257 (*N*-
106 (adamantan-1-yl)-1-(5-hydroxypentyl)-4-methyl-5-phenyl-1H-pyrazole-3-carboxamide), designed
107 by the same authors through an evolutive optimization of Rimonabant, the first known CB1R
108 antagonist approved for clinical use.[72] The visual inspection of the complex allowed the
109 characterization of the binding pocket and provided valuable information on the activation
110 mechanism.[71] Noteworthy, the chemical scaffold of AM10257 consists of a core represented by a
111 pyrazole ring substituted with three groups extending in different directions ("three-arm pose
112 interactions") (Figure 1A). Accordingly, we tried to propose the same type of interactions on our
113 anthranil amide derivatives as shown in Figure 1.
114

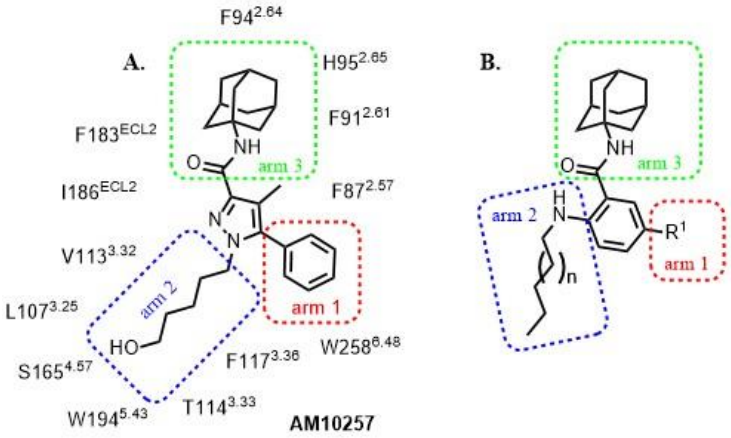

Figure 1. Comparison between the "three-arms pose interactions" of the CB2R antagonist AM10257 within the CB2R binding pocket[71] (A) and the general structure of our *N*-adamantyl-anthranil amide derivatives (B).

Compounds of our series **4-21** (cfr Schemes 1 and 2) replace the pyrazole with the phenyl leaving unchanged the directions of the three decorating groups in agreement with the "three-arms pose interaction" hypothesis. In this respect, the arm 1 can be a hydrogen atom, a bromine atom or an aromatic or heteroaromatic ring. We observed that the phenyl group represented the best option to engage the CB2R and thus we explored electron withdrawing/donating substituents to assess their impact on binding. As far as arm 2 is concerned, the aniline nitrogen atom was alkylated with a variable alkyl chain (five to seven carbon atoms) to evaluate the optimal length for the interaction. With regard to arm 3, the *N*-adamantyl carboxamide group was kept unmodified for its crucial role in establishing hydrophobic interactions with CB2R[54]. To prove the actual importance of the adamantyl group[52,73–75] we also prepared compound **25** (Table 3), which bears, instead, a cyclohexyl ring. All the newly synthesized derivatives were tested for their pharmacodynamic profile (affinity and selectivity at the CB2R) and for the best compounds of the series, in terms of CB2R affinity and selectivity, the CB2R functional profile (agonism or antagonism) was assayed. Importantly, the

impact on the production of the pro- and anti-inflammatory cytokines in monocytes and macrophages, in resting and lipopolysaccharide (LPS) -activated state, was finally evaluated to better support the therapeutic potential of the most promising CB2R ligands as anti-inflamamtory agents.

Chemistry. The synthesis of our *N*-adamantyl-anthranil amide derivatives was accomplished as depicted in Schemes 1–3.

The starting anthranilic acids (commercially available anthranilic acid and **1**) after activation with HBTU, were coupled with adamantylamine in presence of *N*,*N*-Diisopropylethylamine (-DIPEA) in dry dimethylformamide (DMF) affording adamantylamides **2** and **3**, that subsequently provided the corresponding *N*-adamantylanthranil amide derivatives (**4–9**) through a reductive amination with the appropriate aliphatic aldehyde. Scheme 1.

Scheme 1. Synthesis of *N*-adamantylanthranil amide derivatives (4–9)[a]

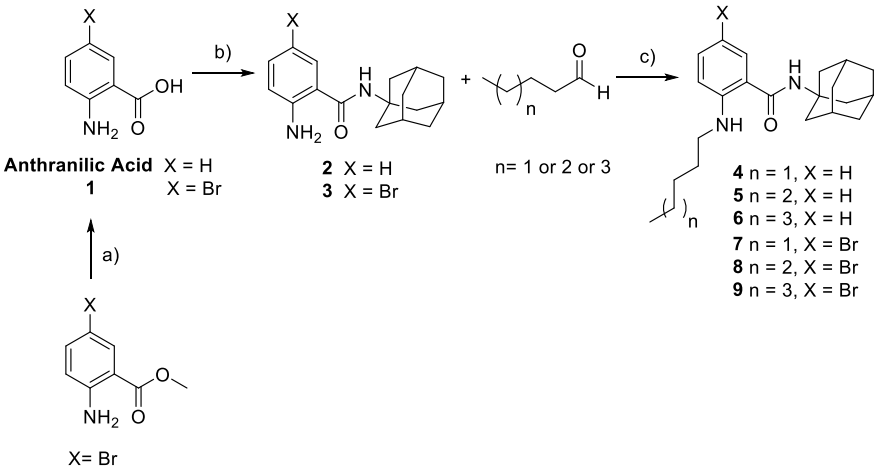

[a]Reagents and conditions: (a) NaOH/EtOH, rt. (b) DIPEA, DMF anhydrous, 0 °C, HBTU, 1-adamantylamine, rt. (c) Aliphatic aldehyde, $NaBH(OAc)_3$, dry THF rt.

As shown in Scheme 2, aryl substituted derivatives of *N*-adamantyl-anthranil amide (**10–21**) were prepared by a Suzuki-Miyaura reaction in dioxane/K_2CO_3 (2M) from the *N*-adamantyl-bromoanthranil amide derivatives (**7–9**) and the appropriate boronic acid.

Scheme 2. Synthesis of substituted derivatives of *N*-adamantyl-anthranil amide (10–21)[a]

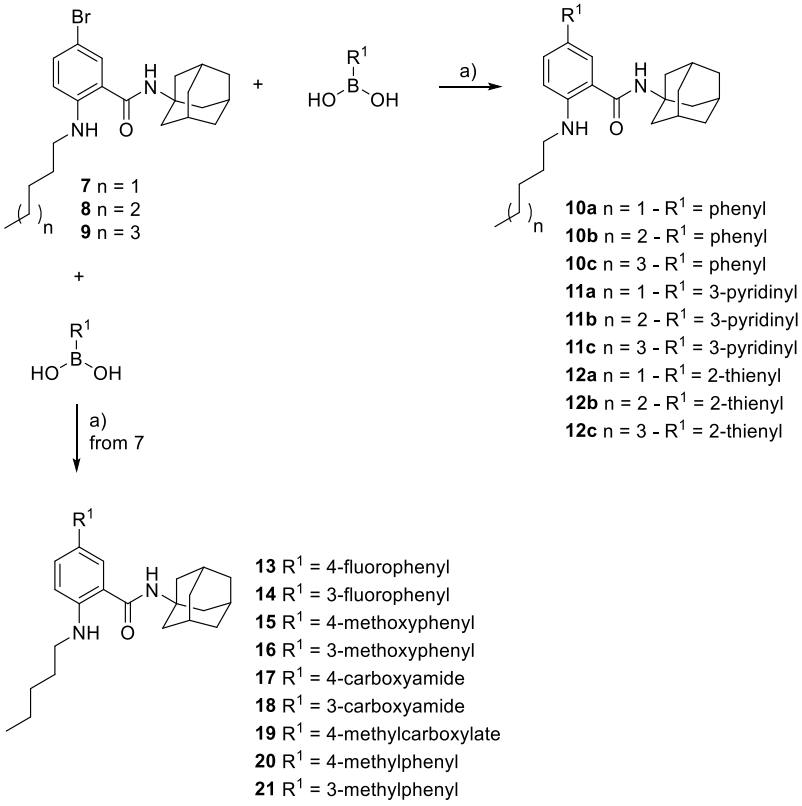

[a]Reagents and conditions: (a) appropriate boronic acid, $Pd(PPh_3)_4$, dioxane/K_2CO_3 (2M), reflux.

The synthesis of derivative **25** was performed from the commercially available methyl-2-amino-5-bromobenzoate that was coupled with benzene boronic acid in dioxane/K_2CO_3 (2M) obtaining compound **22** that upon reductive amination with valeraldehyde gave the *N*-pentil-bromoanthranil amide derivative **23**. Then the ester function was hydrolyzed under basic condition to provide the corresponding carboxylic acids **24** that was coupled with cyclohexylamine in dry DMF leading to the formation of compound **25**. (Scheme 3).

Scheme 3. Synthesis of *N*-cyclohexyl-anthranil amide derivative (25)[a]

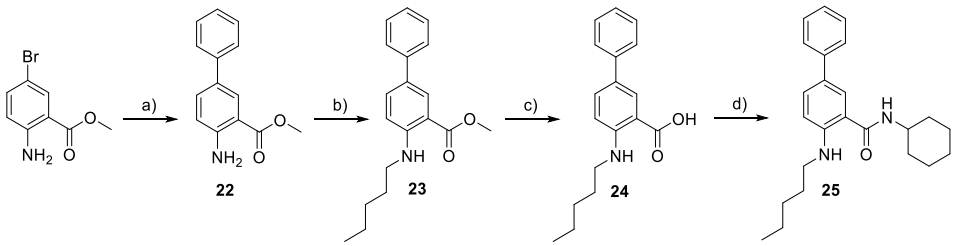

[a]Reagents and conditions: (a) phenylboronic acid, $Pd(PPh_3)_4$, dioxane/K_2CO_3 (2M), reflux. (b) valeraldehyde, $NaBH(OAc)_3$, dry THF, rt. (c) NaOH/EtOH, rt. (d) DIPEA, DMF anhydrous, 0 °C, HBTU, 1-cyclohexylamine, rt.

All reactions were monitored by thin-layer chromatography (TLC). After completion of the reaction, the solvent was evaporated to dryness and the isolated solid was purified by column chromatography on silica gel. A detailed description of the synthetic methods and the complete structural, spectroscopic, and analytical data for all compounds are provided in the experimental part.

Biological Evaluation. All the compounds were tested by radioligand binding assay in order to measure their CB2R affinity profile (reported as K_i value) and their selectivity by testing the affinity at the other cannabinoid receptor subtype, CB1R (reported as % displacement at 1μM). Compounds exhibiting the best pharmacodynamic profile in terms of CB2R affinity (**4**, **10a**, **11a**, **12c** -and **14**) for each R^1 sub-group were also evaluated for the functional behavior (agonism or antagonism) through

cAMP-based assays. ~~Only in the case of the R^1= 2-thienyl we decided to test **12a** instead of **12c** as to fix R^2 as a pentyl chain for all the sub-groups.~~ Moreover, the modulation of the pro- and anti-inflammatory cytokines production was also investigated to exert the ability of the best compounds, **4** and **10a,** to modulate the inflammatory cascade proper of the above mentioned diseases.

Computational Studies. Compounds **4** and **10a** were subjected to molecular docking simulations. This study employed as protein structures both the available X-ray solved crystals of CB2R that are the complex with the agonist (PDB code: 6KPC, released in 2020)[4] and the complex with the antagonist (5ZTY, released in 2019).[71]

RESULTS AND DISCUSSION

As reported in Table 1, the designed series of *N*-adamantyl-anthranil amides returned interesting results in terms of affinity and selectivity towards CB2R. All the compounds are very selective towards CB2R, showing very poor affinity for CB1R.

Table 1. Chemical Structure and CB1R/CB2R Affinity Values of the *N*-adamantyl-anthranil amide ~~Derivatives~~ derivatives 4–21 and 25.

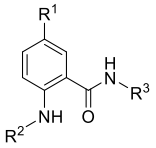

Compounds	R^1	R^2	R^3	CB2R, K_i[a] nM ± SEM or %@ 1μM	CB1R, K_i[b] nM ± SEM or %@ 1μM ~~CB1R, K_i nM ± SEM or %@ 1μM[b]~~

Formattato: Barrato

Formattato: Tipo di carattere: Grassetto

Formattato: Tipo di carattere: Grassetto

Formattato: Tipo di carattere: Grassetto

Formattato: Tipo di carattere: Grassetto

Formattato: Tipo di carattere: Grassetto

4	H	Pentyl	Adamantyl	55.7 ±10.2	31%
5	H	Hexyl	Adamantyl	485.2 ±15.0	6%
6	H	Heptyl	Adamantyl	922.5 ±77.0	4%
7	Br	Pentyl	Adamantyl	455.7 ±20.0	5%
8	Br	Hexyl	Adamantyl	26%±1	17%
9	Br	Heptyl	Adamantyl	16% ±3	8%
10a	Phenyl	Pentyl	Adamantyl	47.8 ±7.6	5%
10b	Phenyl	Hexyl	Adamantyl	209.4 ±25	35%
10c	Phenyl	Heptyl	Adamantyl	1180±220	22%
11a	3-pyridyl	Pentyl	Adamantyl	330±50	1%
11b	3-pyridyl	Hexyl	Adamantyl	6500±820	9%
11c	3-pyridyl	Heptyl	Adamantyl	31%	16 %
12a	2-thienyl	Pentyl	Adamantyl	2600±480	15%
12b	2-thienyl	Hexyl	Adamantyl	465±88	32%
12c	2-thienyl	Heptyl	Adamantyl	160±28	7%
13	4-fluorophenyl	Pentyl	Adamantyl	89.5 ±15.0	754 ±68
14	3-fluorophenyl	Pentyl	Adamantyl	71.0±12.2	42%
15	4-methoxyphenyl	Pentyl	Adamantyl	148.1 ±17	23%
16	3-methoxyphenyl	Pentyl	Adamantyl	25 %	28%
17	4-carboxamide	Pentyl	Adamantyl	19%	14 %

18	3-carboxamide	Pentyl	Adamantyl	21%	3 %
19	4-methylcarboxylate	Pentyl	Adamantyl	12%	6%
20	4-methylphenyl	Pentyl	Adamantyl	128.6	16%
21	3-methylphenyl	Pentyl	Adamantyl	37%	14%
25	Phenyl	Pentyl	Cyclohexyl	21%	3%
Rimonabant					9.8 ±1.7
GW405833				6.9±1.3	
AM10257				0.08 ± 0.01	

[a]Cannabinoid CB2R competition binding experiments were carried out with 0.6 nM [3H]-CP55940; [b]Cannabinoid CB1R competition binding experiments were carried out with 1.25 nM [3H]-CP55940.

The model compounds of the series **4,** presenting a hydrogen as R^1, a pentyl chain as R^2 and an adamantly as R^3, showed high affinity for CB2R (K_i = 55.7 nM) and excellent selectivity in the respect of CB1R. Indeed, no affinity towards CB1–R was observed showing a percentage of radioligand displacement around 31% at 1 μM. Among derivatives bearing an aromatic ring as R^1, we evaluated compounds bearing the phenyl, pyridyl and thienyl substituent. Also, in this case we obtained interesting results in terms of CB2R affinity and selectivity in the respect of CB1R: compound **10a** bearing a phenyl as R^1 and a pentyl chain as R^2 showed high affinity for CB2R (K_i =47.8 nM) and outstanding selectivity in the respect of CB1R showing a percentage of radioligand displacement around 5 % at 1 μM.

Considering the R^2 substitution, a decreased affinity was always observed in derivatives bearing an increase in the chain length; this finding was observed in each R^1 subgroup, except for the 2-thienyl derivatives series, where an opposite trend was observed (**12a** R^2= pentyl, CB2R K_i= 2600 nM *vs* **12c** R^2= heptyl CB2R K_i= 160 nM).

However, the best results in terms of CB2R affinity were obtained when R^2 linked to the aniline nitrogen was the pentyl chain.

Regarding the R^1 substituent, the most interesting findings were obtained when R^1= H and R^1= Phenyl in the derivatives bearing as arm 2 a pentyl chain (**4** and **10a**), while the introduction of a bromine was deleterious (**7–9**). The introduction of other heterocyclic rings, such as 3-pyridyl (**11a–11c**) or 2-thiophenyl (**12a–12c**), is well tolerated even if the same CB2R affinity observed for the compound **10a** (R^1=phenyl, R^2= pentyl R^3= adamantyl CB2R K_i= 47.8 nM) was not observed anymore. For this reason, we decided to decorate the phenyl ring in R^1, and to assess the effects of easy to add electron-withdrawing (R^1= $CONH_2$, COOEt, F) and electron-donating (R^1= CH_3, OCH_3) substituents, leaving unchanged the pentyl chain and the adamantyl carboxamide at R^2 and R^3, respectively. Disappointingly, this attempt failed in improving the affinity of the lead compound **10a** and only in the case of *para* - and *meta* -fluorine derivatives **13** and **14** good affinity values (K_i= 89.5 nM and 71.0 nM, respectively) were observed. However, **13** and **14** were the least selective of the series (CB1R K_i= 754 nM for compound **13** and for **14,** a percentage of radioligand displacement around 42% at [1 μM] was observed). Well tolerated was, also, the introduction of a methoxy (**15**, CB2R K_i= 148.1 nM) or a methyl group (**20**, CB2R K_i= 128.6 nM) in the *para* position of the phenyl in R^1, even if they showed less affinity than **10a**. As above mentioned, we kept unchanged arm 3 as an adamantyl carboxamide in agreement to previous structure-affinity relationship studies demonstrating the pivotal role of this group on CB2R affinity.[29,76–79] To further confirm the robustness of the choice of the *N*-adamantyl carboxamide as arm 3, we synthesized compound **25** bearing a cyclohexyl carboxamide. As expected, a total loss of the CB2R affinity was observed, being the cyclohexyl ring less prone to establish hydrophobic interactions.

Functional Assay. cAMP assays have been performed on the derivatives of each R^1 subgroup showing the best CB2R affinity **(4**, **10a**, **11a**, **12c** and **14**, K_i= 55.7, 47.8, 330, 160 and 71.6 nM, respectively), to evaluate their functional behavior (agonism or antagonism). ~~Only in the case of the R^1= 2-thienyl we decided to test **12a** (CB2R K_i= 2600 nM), instead of **12c** (CB2R K_i= 160 nM) to~~

~~compare ligands with a fixed R^2 as a pentyl chain for all the sub-groups.~~ As depicted in Figure 5, the assay demonstrated a different functional profile for the five ligands: **4**, **11a**, ~~**12a**~~ **12c** and **14** were found to be ~~a~~ CB2R full agonists [being able to block the cAMP production induced by forskolin-derivative NKH-477 (Figure 5)], while compound **10a** was not able to exert this activity. Therefore, **10a** was tested in presence of the CB2R agonist JWH-133 to verify its ability to reverse an agonist-mediated cAMP reduction, thus confirming a CB2R antagonist profile (Figure 2).

Table 2 reports the activity for all the tested compounds and the EC_{50} and the E_{max} values for the agonists; Figure 2 reports the dose-response curves for the two most promising compounds **4** and **10a**.

Table 2. CB2R functional activity of the best CB2R ligands.

Compound	CB2R profile	EC_{50}, μM, (Emax, %)
4	Agonist	0.56 (77.16)
10a	Antagonist	-
11a	Agonist	10.42 (98.13%)
12c~~a~~	Agonist	~~4.13~~5.60 (75.0~~89.97~~%)
14	Agonist	5.25 (86.56%)
JWH-133	Agonist	168.6 (97.50)

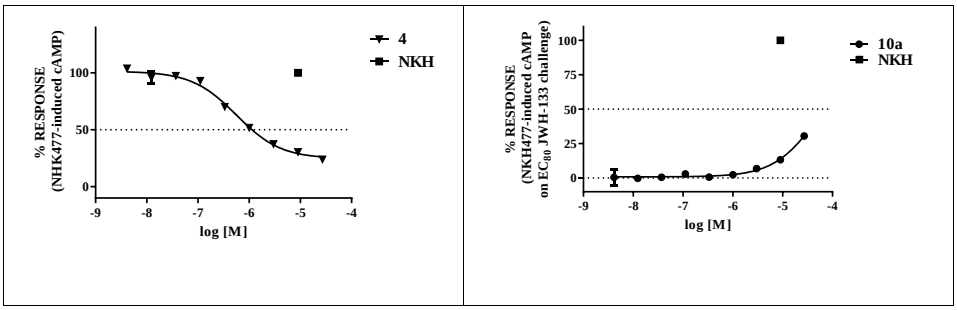

Figure 2. In vitro Biological evaluation of the CB2R functional profile. Concentration-response curves of the two best compounds **4** and **10a** in the cAMP assay. The curves show the effect of increasing concentrations of compounds on NKH-477-induced cAMP levels in stable CHO cells expressing the human CB2R. Data are reported as means ± SEM of three independent experiments conducted in triplicate and normalized for NKH-477 considered as 100% of response.

Computational Studies. With the aim to unveil the molecular rationale behind the experimental data measured for **4** and **10a**, characterized by the best CB2R affinity (55.7 and 47.8 nM respectively) but different functional profile (agonist or antagonist respectively), retrospective docking studies were carried out. As CB2R target for docking, the two recently X-ray solved structures of CB2R complexed with an antagonist (PDB code: 5ZTY, released in 2019)[71] and an agonist (PDB code: 6KPC, released in 2020)[4] were employed .

Noteworthy, the latter was recently proved to be appropriate for reliable docking simulations[80] based on data returned by three benchmark datasets.

A preliminary visual inspection of the binding sites (5ZTY *vs* 6KPC) reveals a substantial overlap with a significant difference concerning the orientation of the indole ring of the W258 side-chain only (compare Figures 3A *vs* 3B). On the other hand, this observation is consistent with the available literature[81] putting forward the conformation of W258 side-chain as crucial for discerning CB2R agonists from antagonists. Figures 3A and 3B show the top-scored docking poses experienced by **10a** within the antagonist and agonist binding sites, respectively. On one hand, **10a** can extend its arm 1, which is a phenyl, to establish pi-pi interactions with both W258 and F117 residues of the antagonist CB2R binding site (5ZTY). On the other, **10a** flips its arm 1 with arm 2 (i.e., the phenyl with pentyl) to fit the agonist CB2R binding site (6KPC) due to the steric hindrance of W258; the strength of this different posing is however supported by the occurrence of a pi-pi interaction engaged by arm 1 with F183. These diverse posing reflect different MM-GBSA binding energies (-120.28 kcal/mol *vs* -116.84 kcal/mol for **10a** in 5ZTY and 6KPC, respectively). Taken as a whole, this analysis would

suggest that compound **10a** might act as a CB2R antagonist. This hypothesis is further supported by the evidence that the detected binding mode in 5ZTY is consistent with that of the cognate antagonist ligand AM10257 (Figure 4).

Unlike **10a**, **4** returns similar top-scored docking poses in 5ZTY and 6KPC. Nevertheless, the slightly different orientations of both F117 and F87 allow **4** establishing two well-oriented pi-pi interactions only when the protein structure complexed with an agonist is taken into account (Figure 3D). This observation is supported by the computed MM-GBSA binding energies, being equal to -98.57 kcal/mol when 5ZTY is used as protein structure and -108.82 kcal/mol when 6KPC is employed. As a result, the performed docking simulations indicate that, despite their very similar chemical structure, **4** and **10a** might be responsible for opposite CB2R activities. **10a**, indeed, behaves, within the CB2R pocket, as the antagonist AM10257, establishing key interactions with W258 and F117,[71] while **4** perfectly reproduces the binding mode of the agonist AM12033, being able to establish a pi-pi interaction with F87 in a cavity position distant from W258.[71,81]

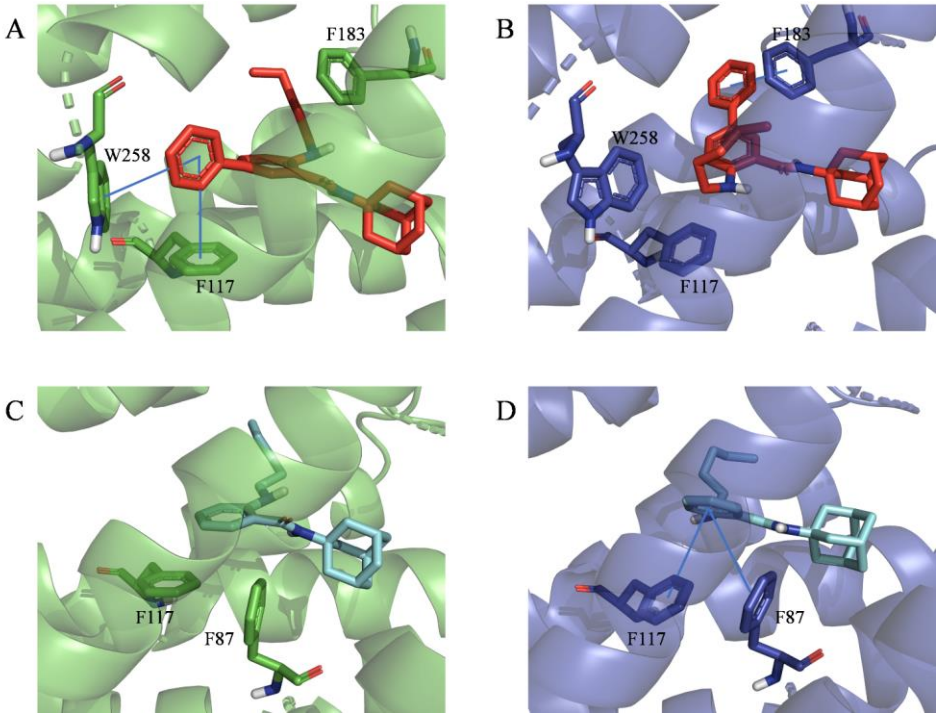

289

290 **Figure 3.** Top-scored docking poses returned by docking simulations performed on **10a** (A, B) and **4**

291 (C, D).

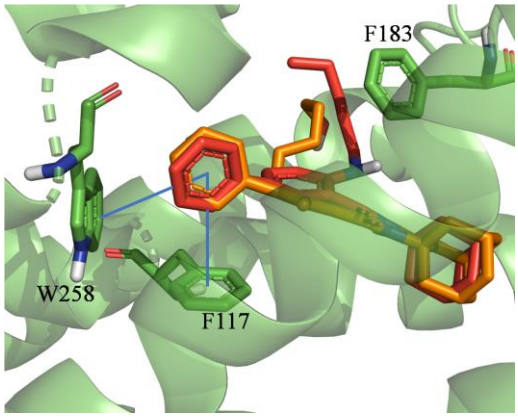

292 **Figure 4.** Alignment between the top-scored docking pose returned by docking simulations
293 performed on **10a** ~~(ASF136)~~ (red) and the co-x antagonist ligand AM10257 (orange) Ligands and

important residues are rendered as sticks, whereas the 5ZTY (green) and 6KPC (violet) proteins are represented as a cartoon. Pi-pi interactions are indicated by solid blue lines. For the sake of clarity, only polar hydrogen atoms are shown.

Cytokines production. In order to study the potential of our ligands for the treatment of pathologies etiologically related to inflammation (e.g, cancer, neurodegeneration but also obesity or NAFLD), we tested the impact of the two compounds **4** and **10a,** displaying the highest CB2R affinity and opposite profile as CB2R agonist and antagonist, respectively, on the production of the pro-inflammatory (TNF-α, IFN-γ, IL-1β and IL-6) and anti-inflammatory (IL-4 and IL-10) cytokines, in monocytes and macrophages, in basal and LPS-activated state. The induced effects were also compared to that of the CB2R reference agonist CB65[82] and antagonist JTE907,[83] as well as in co-administration assays where, the agonist **4** and the antagonist **10a** were co-incubated with the CB2R antagonist JTE907 and agonist CB65, respectively.

Preliminary studies (data not shown) led us to use for each reference compound 10μM as test concentration since at this dose CB65 exerted its maximal effect on cytokines production and JTE097 was not active.

Figure 5 reports the activity exerted by the CB2R agonist **4,** at 1 and 10μM (2- and 10-fold its EC_{50}), alone and in the presence of the CB2R antagonist JTE907 (10 μM) in order to define the CB2R contribution in the observed effect. The effect induced by compound **4** was also compared to that of the CB2R reference agonist CB65 (10μM).

As depicted in panel A, in resting monocytes, compound **4** decreased the production of the pro-inflammatory cytokines (TNF-α, IFN-γ, IL-1β and IL-6) and increased the production of the anti-inflammatory ones (IL-10 and IL-4) in a dose-dependent manner. The observed behavior at 10μM was comparable (even if with a lower extent) to that of the CB2R reference agonist CB65. More specifically, CB65 induced a 60% reduction in TNF-α, IL-1β and IL-6 and 40% reduction in IFN-γ production, while compound **4** at 10 μM induced a 50% reduction in TNF-α, IFN-γ, IL-1β and 40%

reduction in IL-6 production. As for the anti-inflammatory cytokines, CB65 and compound **4** at 10 μM led to a comparable increase in IL-4 and IL-10 production. The same trend was detected and more evident in activated-monocytes, incubated with both the CB2R agonists CB65 and **4** at 10μM, as depicted (Figure 5, panel B).

The activity of both CB65 and **4** was reverted by the CB2R inverse agonist JTE907, thus unequivocally demonstrating the CB2R-mediated effect.

In resting macrophages, CB65 and compound **4** showed a comparable decreased production of the pro-inflammatory cytokines (50-60% reduction) and an increased production of the anti-inflammatory cytokines (Figure 5, panel C), while the effect was more pronounced in activated-macrophages (Figure 5, panel D). Both CB65 and compound **4** induced a 70-80% reduction in the pro-inflammatory cytokines and significant increased IL-4 and IL-10 production. Also in these cases, the effect of both the CB2R agonists was reverted by JTE907.

A

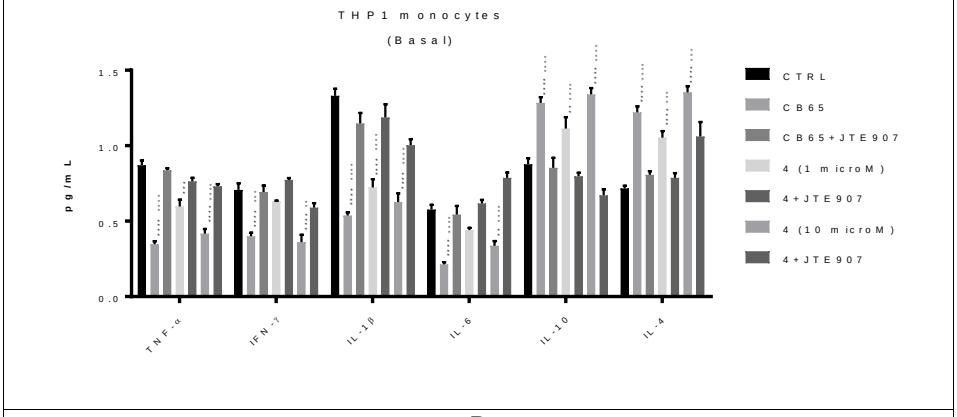

B

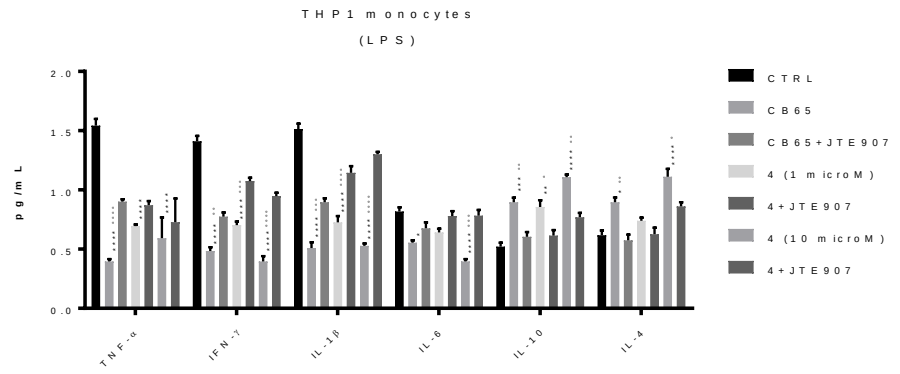
THP1 monocytes
(LPS)
pg/mL
2.0
1.5
1.0
0.5
0.0
TNF-α
IFN-γ
IL-1β
IL-6
IL-10
IL-4
CTRL
CB65
CB65+JTE907
4 (1 microM)
4+JTE907
4 (10 microM)
4+JTE907

C

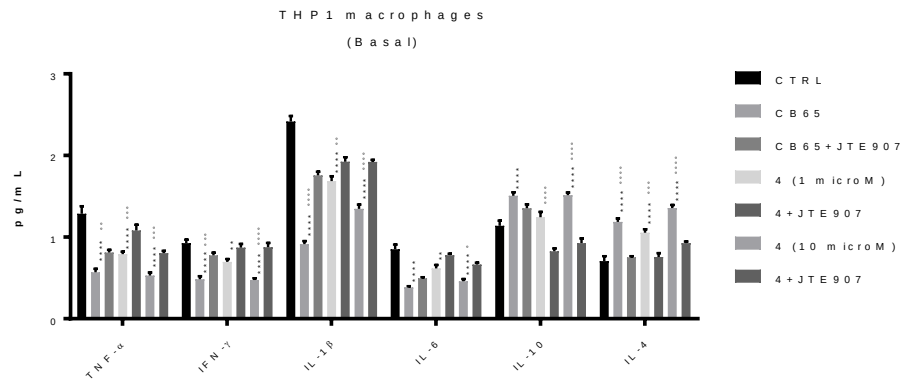
THP1 macrophages
(Basal)
pg/mL
3
2
1
0
TNF-α
IFN-γ
IL-1β
IL-6
IL-10
IL-4
CTRL
CB65
CB65+JTE907
4 (1 microM)
4+JTE907
4 (10 microM)
4+JTE907

D

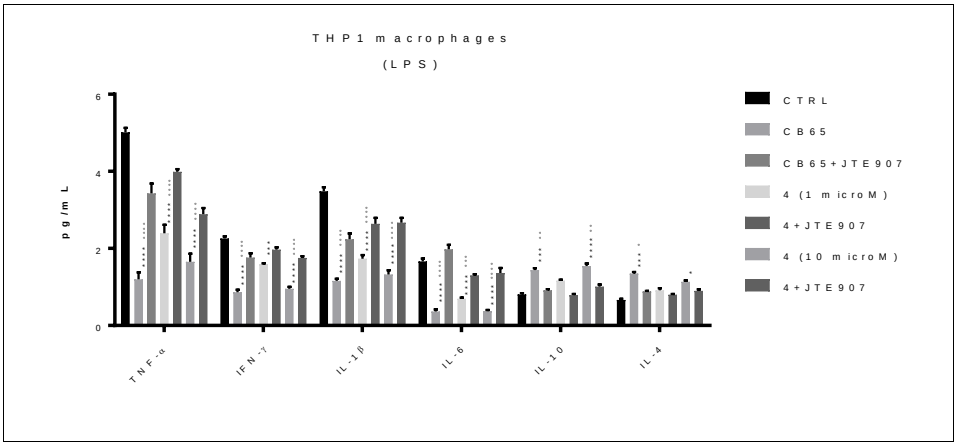

Figure 5. Cytokine levels in human monocytes (A, B) and macrophages (C, D) in resting (basal) and activated (LPS) conditions by treatment with the CB2R agonist reference compound CB65 (10 μM) and the CB2R agonist compound **4** (at 1 and 10 μM), alone and in the presence of the CB2R antagonist JTE907 (10μM).

[a]THP-1 cells, treated or not with 0.01 μM PMA for 48 h to differentiated them into macrophages, were incubated for additional 24 h in the absence or presence of 10 μg/ml LPS, without (CTRL) or with the CB2R ligands **4** and **CB65**, in the absence and in the presence of the CB2R antagonist JTE907. Cytokines levels were measured with an ELISA coupled with qRT-PCR. Each bar represents the mean ± SEM of two experiments performed in triplicate. Two-Way ANOVA followed by Tukey post-hoc test was applied. Significance of symbols as follows: 1 symbol=p<0.05; 2 symbols= p<0.01; 3 symbols =p<0.001; 4 symbols=p<0.0001. Legend for symbols as follows: * indicates *vs* CTR; ° indicates *vs* each compound with JTE907.

Commentato [RGC2]: Questo sarebbe il controllo? Forse dobbiamo aggiungere prima la parola per intero e poi l'abbreviazione

Commentato [RGC3]: Questo e' lo stesso del CTRL di sopra?

Figure 6 reports the impact of the CB2R antagonist, compound **10a,** alone and in the presence of the CB2R reference agonist CB65, on the cytokines production. As evident in all the panels compound **10a**, analogously to the CB2R reference antagonist JTE907, has an impact on the cytokines production opposite to that of the agonist compound **4**, and -importantly - it reversed the effects induced by the CB2R agonist CB65, both in monocytes and macrophages in resting and activated condition.

These findings support the different CB2R activity profile of the two new compounds **4** and **10a** as CB2R agonist and antagonist, respectively.

355

A

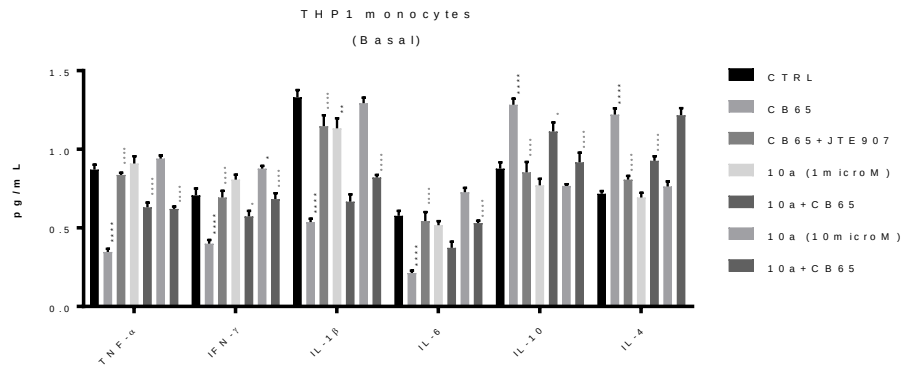
THP1 monocytes
(Basal)
pg/mL
1.5
1.0
0.5
0.0
TNF-α
IFN-γ
IL-1β
IL-6
IL-10
IL-4
CTRL
CB65
CB65+JTE907
10a (1microM)
10a+CB65
10a (10microM)
10a+CB65

B

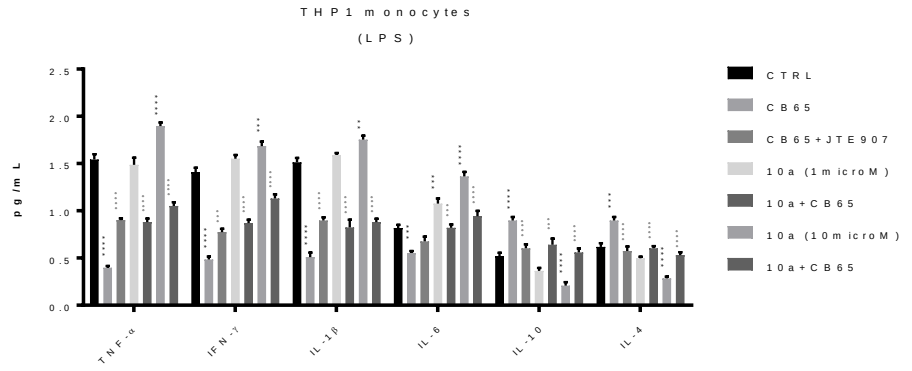
THP1 monocytes
(LPS)
pg/mL
2.5
2.0
1.5
1.0
0.5
0.0
TNF-α
IFN-γ
IL-1β
IL-6
IL-10
IL-4
CTRL
CB65
CB65+JTE907
10a (1microM)
10a+CB65
10a (10microM)
10a+CB65

C

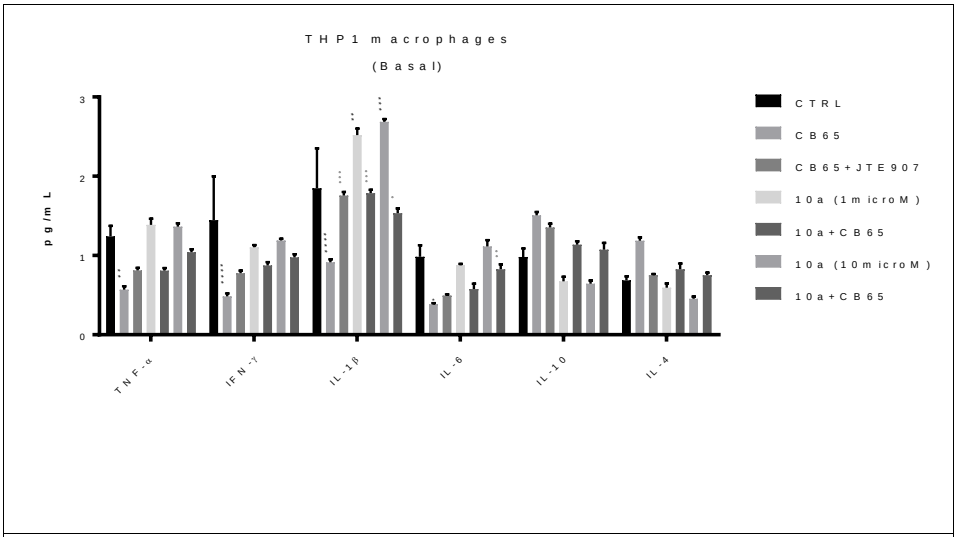

D

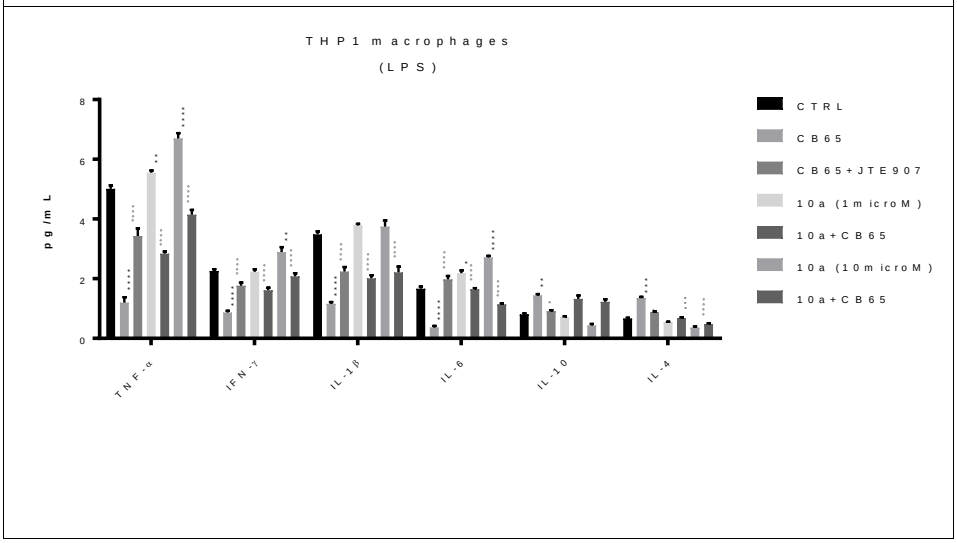

Figure 6. Cytokine levels in human monocytes (A, B) and macrophages (C, D) in resting (basal) and activated (LPS) conditions by treatment with the CB2R agonist reference compound CB65 (10 μM) alone and in the presence of the CB2R antagonist JTE907 (10μM) and in the presence of the CB2R antagonist compound **10a** (at 1 and 10 μM).

[a]THP-1 cells, treated or not with 0.01 μM PMA for 48 h to differentiated them into macrophages, were incubated for additional 24 h in the absence or presence of 10 μg/ml LPS, without (CTRL) or with the CB2R ligands **10a** and **CB65**, in the absence and in the presence of the CB2R agonist CB65 and CB2R antagonist JTE907, respectively. Cytokines levels were measured with an ELISA coupled with qRT-PCR. Each bar represents the mean ± SEM of two experiments performed in triplicate.

Two-Way ANOVA followed by Tukey post-hoc test was applied. Significance of symbols as follows: 1 symbol=p<0.05; 2 symbols= p<0.01; 3 symbols =p<0.001; 4 symbols=p<0.0001. Legend for symbols as follows: * indicates *vs* CTR; ° indicates *vs* CB65.

Statistical analysis. All data in the text and figures are provided as means ± SEM. The results were analysed by Two-way ANOVA test, using Graph-Pad Prism (Graph-Pad software, San Diego, CA, USA). $p < 0.05$ was considered significant.

CONCLUSION

In this work, we rationally designed and synthesized new *N*-adamantyl-anthranil amide derivatives and evaluated their affinity and selectivity profiles towards CB2R. Our derivatives displayed affinity in the nanomolar range for human CB2R as well as an excellent selectivity. Based on the "three-arms pose interactions" hypothesis, our efforts aimed to find suitable substituents to optimize affinity and selectivity. We found that the CB2R binding site can be effectively targeted if: a hydrogen atom (**4**) or a phenyl ring (**10a**) is employed as arm 1; a pentyl chain is present as arm 2; and an adamantly carboxamide represents arm 3.

Based on a combined experimental/computational study, we explain how the CB2R agonism/antagonism switch of our *N*-adamantyl-anthranil amide derivatives is causatively related to the chance of making pi-pi interactions with W258 side-chain. Molecular docking provided a molecular rationale by highlighting the importance of substituents on arm 1.

To achieve this aim, comparative docking simulations were performed on both the recently published CB2R crystal structures, one complexed with an agonist and the other with an antagonist and we were able to understand the functional activity of our compounds evidencing how the introduction of a phenyl ring on arm 1 could be responsible for an agonism/antagonism switch resulting from the establishment of pi-pi interactions with W258.

Therefore, we also remark the reduced production of the pro-inflammatory cytokines induced by CB2R agonist compound **4** that could be considered as a new therapeutic option for diseases characterized by a strong inflammatory response such as COVID-19. Moreover, the identification of

compound **10a** as CB2R antagonist opens a new scenario in the development of CB2R antagonist as tools to give new piece of information about the application of also this class of CB2R ligands.

EXPERIMENTAL SECTION

Chemistry. High analytical grade chemicals and solvents were purchased from commercial suppliers. When necessary, solvents were dried by standard techniques and distilled. After extraction from aqueous phases, the organic solvents were dried with anhydrous sodium sulphate. Thin layer chromatography (TLC) was performed on aluminum sheets precoated with silica gel 60F254 (0.2 mm) (E. Merck, Darmstadt, Germany). Chromatographic spots were visualized by UV light. Purification of crude compounds was carried out by flash column chromatography on silica gel 60 (Kieselgel 0.040–0.063 mm; E. Merck) or gravitational chromatography column on silica gel 60 (Silicagel 0,063-0,200 mm, E. Merck) or by preparative TLC on silica gel 60 F254 glass plates. Melting points (mp) were determined with a capillary apparatus (Büchi 540). ^{1}H NMR spectra were recorded in DMSO-d_6 or $CDCl_3$ at 300 MHz on a Varian Mercury 300 instrument or on a 500-vnmrs500 spectrometer (500 MHz). ^{13}C NMR (126 MHz) were recorded on a 500-vnmrs500 spectrometer (500 MHz) on novel final compounds. Chemical shifts (δ scale) are reported in parts per million (ppm) relative to the central peak of the solvent. Coupling constant (J values) are given in Hertz (Hz). Spin multiplicities are given as s (singlet), br s (broad singlet), d (doublet), t (triplet), dd (double doublet), dt (double triplet), q (quartet), quint (quintet) or m (multiplet). LRMS (ESI) was performed with an electrospray interface ion trap mass spectrometer (1100 series LC/MSD trap system: Agilent, Palo Alto, CA, USA). In all cases, spectroscopic data agree with compounds and assigned structures. The purity of target compounds listed in table ST1 in the supplementary material was assessed by HPLC. Analytical HPLC analyses were performed on an Agilent 1260 Infinity (Agilent Technologies, Palo Alto, CA, USA) equipped with a quaternary pump (G1311C), a membrane degasser, an autosampler (G1329B), a diode-array detector (DAD) (G1315D). Data analyses were processed by HP ChemStation system (Agilent Technologies). The analytical column

was a reversed phase column (Phenomenex Kinetex C-18, 5 µm, 100 Å, 150 × 4.6 mm). All compounds were dissolved in the mobile phase at a concentration of about 1 mg/mL and injected through a 5 mL loop. Isocratic elution was conducted at a flow rate of 1 mL/min with MeOH/H_2O (85:15, v/v), unless otherwise stated. UV signal was detected at 266 nm, 294 nm, and 330 nm. All compounds showed >96% purity.

Synthesis of 2-amino-5-bromobenzoic acid 1. The methyl-2-amino-5-bromobenzoate (0.23 g, 1.0 mmol) is dissolved in a 1:1 solution of NaOH (2N) (8 mL) and absolute EtOH (8 mL). The reaction mixture is left at room temperature and under magnetic stirring for 4 hours. The solution is then acidified with HCl (3N) until a precipitate is formed (pH = 4/5). The product is recovered by filtration and washed with water at pH = 4. The product is extracted with CH_2Cl_2 (DCM) (3x10 mL), and the organic phases are combined and dried over Na_2SO_4. The solvent is removed under reduced pressure obtaining 2-amino-5-bromobenzoic acid **1**. Yield: 90%. ^{1}H NMR (300 MHz, DMSO-d_6) δ: 8.58 (s br, 2H), 7.72 (d, J = 2.9 Hz, 1H), 7.33 (dd, J_1 = 9.0, J_2 = 2.9 Hz, 1H), 6.71 (d, J = 9.0 Hz, 1H). ESI-MS: m/z 214 $[M-H]^-$.

General procedure for the synthesis of *N*-(adamantan-1-yl)-2-aminobenzammides 2 and 3. The appropriate anthranilic acid (17.0 mmol) was placed in a reaction flask, previously dried under argon, and dissolved in anhydrous DMF (50.0 mL). DIPEA (9.0 mL) was added at 0 °C, and the mixture is left under magnetic stirring at 0 °C for 10 minutes. HBTU (9.67 g, 25.5 mmol) was added to the solution and the mixture is left at room temperature for 2 hours. Then,1-adamantylamine (3.86 g, 25.5 mmol) was added to the solution. The system was left under stirring overnight at room temperature. The solvent was evaporated, and brine (20 mL) was added to the residue that was extracted with methylene chloride (3x 20 mL). The organic layer was washed with HCl 1N (3x20 mL), then with a saturated solution of $NaHCO_3$ (3x20 mL) and brine (3x20 mL). The organic layer was dried over anhydrous Na_2SO_4, filtered and evaporated. The resulting crude product was purified by gravitational gradient chromatography column (n-hexane/ethyl acetate: 9/1 to 8/2) obtaining the desired intermediate.

***N*-(adamantan-1-yl)-2-aminobenzammides 2.** Yield: 71%. ^{1}H NMR (300 MHz, $CDCl_3$) δ= 7.25 (s,1H), 7.17 (t, *J* = 5.2 1H), 6.66-6.61 (m, 2H), 5.70 (s br, 1H), 5.39 (s br, 2H), 2.15–2.09 (m, 9H), 1.75–1.69 (m, 6H). ESI-MS: m/z 293 $[M+Na]^+$.

***N*-(adamantan-1-yl)-2-amino-5-bromobenzamide 3.** Yield: 77%. ^{1}H-NMR (300 MHz, $CDCl_3$) δ: 7.34 (d, *J* = 2.2 Hz, 1H), 7.24 (dd, *J* = 8.7 Hz, 2.2 Hz, 1H), 6.54 (d, *J* = 8.7 Hz 1H), 5.62 (s br, 1H), 5.39 (s br, 2H), 2.17–2.05 (m, 9H), 1.76–168 (m, 6H). ESI-MS: m/z 371 $[M+Na]^+$.

General procedure for the synthesis of *N*-adamantyl-anthranilamide derivatives 4–9. In a dried reaction flask, the appropriate intermediate **2** or **3** (0.37 mmol) was suspended in anhydrous THF (10 mL). The appropriate aliphatic aldehyde (0.8 mmol) was added and the mixture was left under magnetic stirring 3 h at room temperature. Later, $NaBH(OAc)_3$ (0.16 g, 0.74 mmol) was added at 0 °C to the mixture and the solution is left under magnetic stirring overnight at room temperature. After the addition of methanol (MeOH) (5 mL), the solvent was removed under reduced pressure. The resulting residue was purified by gradient gravitational column chromatography (eluent: n-hexane/ethyl acetate: 9.5/0.5 to 9 /1) to obtain the final compounds **4–9**.

***N*-(adamantan-1-yl)-2-(pentylamino)benzamide 4.** Yield: 47%. mp: 122-123 °C. ^{1}H NMR (500 MHz, $CDCl_3$) δ: 7.27-7.23 (m, 2H), 6.65 (d, *J* = 8.0 Hz 1H), 6.53 (td, *J* = 6.5, 1.1 Hz 1H), 5.69 (s br, 1H), 3.11(q, *J* = 5.5 Hz, 2H) 2.18–2.08 (m, 9H), 1.75–1.65 (m, 8H), 1.41–1.32 (m, 4H), 0.91 (t, *J* = 7.0 Hz 3H). ^{13}C-NMR (126 MHz, $CDCl_3$) δ: 169.46, 149.51, 132.18, 127.26, 116.79, 114.17, 111.44, 52.12, 43.15, 41.75, 36.40, 29.50, 29.43, 28.94, 22.49, 14.02. ESI-MS: m/z 363 $[M+Na]^+$.

***N*-(adamantan-1-yl)-2-(hexylamino)benzamide 5.** Yield: 32%. mp: 103-104°C. ^{1}H NMR (500 MHz, $CDCl_3$) δ: 7.27-7.24 (m, 3H), 6.65 (d, *J* = 8.1 Hz, 1H), 6.53 (td, *J* = 6.9, 1.1 Hz, 1H), 5.69 (s br, 1H), 3.11 (q, *J* = 4.5 Hz, 2H) 2.15–2.06 (m, 9H), 1.75–1.62 (m, 8H); 1.42–1.28 (m, 2H), 1.30–1.34 (m, 4H), 0.89 (t, *J* = 7.0 Hz, 3H). ^{13}C-NMR (126 MHz, $CDCl_3$) δ: 169.45, 149.51, 132.18, 127.25, 116.80, 114.17, 111.44, 52.12, 43.18, 41.75, 36.40, 31.62, 29.50, 29.20, 26.94, 22.58, 14.03. ESI-MS: m/z 377 $[M+Na]^+$.

***N*-(adamantan-1-yl)-2-(heptylamino)benzamide 6.** Yield: 36%. mp: 94-95 °C. ^{1}H NMR (500 MHz, $CDCl_3$) δ: 7.27-7.24 (m, 3H), 6.65 (d, J = 8.5 Hz, 1H), 6.53 (td, J = 6.9, 1.1 Hz, 1H), 5.69 (s br, 1H), 3.11 (q, J = 4.5 Hz, 2H) 2.15–2.06 (m, 9H), 1.75–1.68 (m, 8H), 1.42–1.28 (m, 8H), 0.88 (t, J = 7.0 Hz 3H). ^{13}C-NMR (126 MHz, $CDCl_3$) δ: 169.45, 149.51, 132.18, 127.25, 116.80, 114.17, 111.45, 52.12, 43.17, 41.75, 36.40, 31.76, 29.50, 29.23, 29.08, 27.21, 22.60, 14.08. ESI-MS: m/z 391 $[M+Na]^+$.

***N*-(adamantan-1-yl)-5-bromo-2-(pentylamine)benzamide 7.** Yield: 51%. mp: 143-144°C. ^{1}H NMR (500 MHz, $CDCl_3$) δ: 7.33 (d, J = 2.5 Hz, 1H), 7.30 (dd, J = 8.5, 2.5 Hz, 1H), 7.72 (s br, 1H) 6.52 (d, J = 9.0 Hz, 1H), 5.62 (s br, 1H), 3.07 (q, J = 7.2 Hz, 2H), 2.12–2.09 (m, 9H), 1.72–1.62 (m, 8H), 1.39–1.33 (m, 4H), 0.91 (t, J = 7.0 Hz, 3H). ^{13}C-NMR (126 MHz, $CDCl_3$) δ: 168.10, 148.37, 134.65, 129.68, 118.46, 113.18, 105.41, 52.46, 43.19, 41.65, 36.34, 29.47, 29.35, 28.76, 22.44, 13.99. ESI-MS: m/z 441 $[M+Na]^+$.

***N*-(adamantan-1-yl)-5-bromo-2-(hexylamine)benzamide 8.** Yield: 70%. mp: 110-111°C. ^{1}H NMR (500 MHz, $CDCl_3$) δ: 7.33 (d, J = 2.4 Hz, 1H), 7.30 (dd, J_1 = 8.8, 2.4 Hz, 1H), 7.72 (s br, 1H) 6.52 (d, J = 8.5 Hz, 1H), 5.61 (s br, 1H), 3.07 (q, J = 7.6 Hz, 2H), 2.12–2.09 (m, 9H), 1.72–1.60 (m, 8H), 1.42–1.28 (m, 6H), 0.89 (t, J = 7.0 Hz, 3H). ^{13}C-NMR (126 MHz, $CDCl_3$) δ: 168.11, 148.37, 134.65, 129.67, 118.46, 113.18, 105.39, 52.46, 43.21, 41.65, 36.34, 31.57, 29.47, 29.03, 26.86, 22.55, 14.00. ESI-MS m/z 431 $[M-H]^-$.

***N*-(adamantan-1-yl)-5-bromo-2-(heptylamine) benzamide 9.** Yield: 89%. Mp: 102-103°C. ^{1}H-NMR (500 MHz, $CDCl_3$) δ: 7.33 (d, J = 2.4 Hz, 1H), 7.30 (dd, J = 8.8, 2.4 Hz, 1H), 6.55 (d, J = 9.0 Hz, 1H), 5.63 (s br, 1H), 3.07 (t, J = 7.5 Hz, 2H), 2.12–2.09 (m, 9H), 1.74–1.59 (m, 8H), 1.42–1.26 (m, 8H), 0.88 (t, J = 7.0 Hz, 3H). ^{13}C-NMR (126 MHz, $CDCl_3$) δ: 168.03, 148.10, 134.68, 129.68, 118.65, 113.49, 52.49, 41.64, 36.34, 31.72, 29.47, 29.03, 29.00, 27.12, 22.58, 14.07. ESI-MS: m/z 469 $[M+Na]^+$.

General procedure for the synthesis of substituted derivatives of *N*-adamantyl-anthranil amide 10–21. Intermediates **3** or **4** or **5** (0.22 mmol) and the appropriate boronic acid (0.34 mmol) are

suspended in a solution of dioxane (2.4 ml) and K_2CO_3 2M (0.6 ml). After purging the solution with N_2 for 10 minutes, $Pd(PPh_3)_4$ (0.025 g, 0.022 mmol) was added and the mixture was refluxed for about 2–4 hours. Then, the solvent was removed under reduced pressure and the resulting residue was purified by a flash column chromatography: for compounds **10a**, **10b** and **10c**: n-hexane/ ethyl acetate 9/1); compounds **11a**, **11b** and **11c** (eluent: n-hexane/ethyl acetate 9/1 to 7.5/2.5); compounds **12a**, **12b** and **12c** (eluent: n-hexane/ ethyl acetate 9.5/0.5); compounds **13** and **14** (eluent: n-hexane/ethyl acetate 9.8/0.2 to 9.5/0.5); compounds **15** and **16** (eluent: n-hexane/ ethyl acetate 9.8/0.2); compounds **17** and **18** (eluent: methylene chloride/ethyl acetate 9/1 to 7/3); compound **19** (eluent: n-hexane/ ethyl acetate 9.8/0.2 to 9.5/0.5); compounds **20** and **21 (**eluent: n-hexane/ethyl acetate 9.8/0.2)

***N*-(adamantan-1-yl)-4-(pentylamino)-[1,1'-biphenyl]-3-carboxamide 10a.** Yield: 50%. mp: 140-141°C. ^{1}H NMR (500 MHz, $CDCl_3$) δ: 7.57–7.52 (m, 3H), 7.48 (d, *J* = 1.5 Hz 1H), 7.41 (t, *J* = 7.5 Hz, 2H), 7.29 (m, 2H), 6.85 (s br, 1H), 5.79 (s br, 1H), 3.18 (t, *J* = 9.8 Hz, 2H), 2.17–2.09 (m, 9H), 1.76–1.68 (m, 8H), 1.43–1.35 (m, 4H), 0.90 (t, J = 7.5 Hz, 1H). ^{13}C-NMR (126 MHz, $CDCl_3$) δ: 169.44, 148.72, 140.88, 130.86, 128.73, 127.37, 126.20, 125.94, 117.37, 111.84, 52.29, 43.26, 41.74, 36.40, 29.51, 29.42, 28.95, 22.49, 14.02. ESI-MS: m/z 439 $[M+Na]^+$.

***N*-(adamantan-1-yl)-4-(hexylamino)-[1,1'-biphenyl]-3-carboxamide 10b.** Yield: 32%. mp: 137-138 °C. ^{1}H-NMR (500 MHz, $CDCl_3$) δ: 7.51 (dd, *J* = 8.0, 1.5 Hz, 3H), 7.46 (d, *J* = 1.5 Hz 1H), 7.41 (t, *J* = 8.0 2H), 7.30–7.28 (m, 1H), 6.73 (d, *J* = 8.0 Hz 1H), 5.75 (s br, 1H), 3.17 (q, *J* = 5.0 Hz, 2H), 2.16–2.10 (m, 9H), 1.76–1.65 (m, 8H), 1.45–1.39 (m, 2H), 1.36–1.29 (m, 4H), 0.90 (t, *J* = 7.0 Hz, 3H). ^{13}C-NMR (126 MHz, $CDCl_3$) δ: 169.43, 148.73, 140.88, 134.65, 130.86, 128.73, 127.33, 126.20, 125.94, 117.33, 111.82, 52.28, 43.26, 41.73, 36.39, 31.62, 29.50, 29.22, 26.93, 22.59, 14.03. ESI-MS: m/z 453 $[M+Na]^+$.

***N*-(adamantan-1-yl)-4-(heptylamino)-[1,1'-biphenyl]-3-carboxamide 10c.** Yield: 55%. mp: 133-134°C. ^{1}H NMR (500 MHz, $CDCl_3$) δ: 7.50 (dd, *J* = 8.5, 1.5 Hz, 3H), 7.46 (d, *J* = 1.5 Hz, 1H), 7.41 (t, *J* = 8.5 Hz, 2H), 7.30-7.28 (m, 1H), 6.74 (d, *J* = 8.5 Hz, 1H), 5.75 (s br, 1H), 3.16 (t, J = 7.0

2H), 2.18–2.07 (m, 9H), 1.76-1.65 (m, 8H), 1.44-1.29 (m, 8H), 0.89 (t, *J* = 7.0 Hz, 3H). ^{13}C-NMR (126 MHz, $CDCl_3$) δ: 169.41, 140.86, 130.86, 128.74, 126.21, 125.93, 111.87, 109.99, 52.29, 41.73, 36.39, 31.76, 29.68, 29.47, 29.23, 29.08, 27.19, 22.61, 14.08. ESI-MS: m/z 443 $[M-H]^-$.

***N*-(adamantan-1-yl)-2-(pentylamino)-5-(pyridin-3-yl)benzamide 11a.** Yield: 42%. mp: 108-109 °C. ^{1}H NMR (500 MHz, $CDCl_3$) δ: 8.78 (s, 1H), 8.50 (d, *J* = 2.0 Hz, 1H), 7.70 (dt, *J* = 8.5, 2.0 Hz, 1H), 7.48 (dd, *J*=8.5, 2.0 Hz, 1H), 7.45 (d, *J* = 2.0 Hz, 1H), 7.34-7.30 (m, 2H), 6.75 (d, *J* = 8.5 Hz, 1H), 5.76 (s br, 1H), 3.16 (q, *J* = 4.5 Hz, 2H), 2.18–2.10 (m, 9H), 1.76–1.67 (m, 6H), 1.44–1.34 (m, 4H), 0.92 (t, *J* = 7.0 Hz, 3H). ^{13}C-NMR (126 MHz, $CDCl_3$) δ: 169.16, 149.26, 147.47, 147.29, 136.30, 133.24, 130.74, 125.94, 123.56, 123.48, 117.54, 112.04, 52.41, 43.16, 41.72, 36.37, 29.49, 29.39, 28.87, 22.47, 14.01. ESI-MS: m/z 416 $[M-H]^-$.

***N*-(adamantan-1-yl)-2-(hexylamino)-5-(pyridin-3-yl)benzamide 11b.** Yield: 86%. mp: 104-105 °C. ^{1}H NMR (500 MHz, $CDCl_3$) δ: 8.76 (s, 1H), 8.50 (d, *J* = 2.0 Hz, 1H), 7.70 (dt, J_2 = 8.5, 2.0 Hz, 1H), 7.48 (dd, , J_1 = 8.5, 2.0 Hz, 1H), 7.44 (d, *J* = 2.0 1H), 7.36-7.30 (m, 2H), 6.75 (d, *J* = 8.5 Hz, 1H), 5.76 (s br, 1H), 3.15 (q, *J* = 4.5 Hz, 2H), 2.18–2.06 (m, 9H), 1.76–1.64 (m, 8H), 1.45–1.39 (m, 2H), 1.34–1.20 (m, 4H), 0.90 (t, *J* = 7.0 Hz, 3H). ^{13}C-NMR (126 MHz, $CDCl_3$) δ: 169.16, 149.25, 147.45, 147.27, 136.30, 133.25, 130.74, 125.94, 123.55, 123.49, 117.56, 112.05, 52.41, 43.19, 41.71, 36.37, 31.59, 29.49, 29.14, 26.89, 22.57, 14.02. ESI-MS m/z 432 $[M+H]^+$.

***N*-(adamantan-1-yl)-2-(heptylamino)-5-(pyridin-3-yl)benzamide 11c.** Yield: 47%. mp: 76-77°C. ^{1}H NMR (500 MHz, $CDCl_3$) δ: 8.76 (d, *J* = 2.0 1H), 8.50 (dd, Hz, *J* = 4.5, 2.0 Hz, 1H), 7.78 (dt, *J* = *J*= 8.5, 2,0 Hz, 1H), 7.48 (dd, *J*= 8.5, 2 Hz, 1H), 7.45 (d, *J* = 2.0 1H), 7.34-7.29 (m, 2H), 6.75 (d, *J* = 8.5 Hz, 1H), 5.75 (sbr, 1H), 3.16 (q, *J* = 6.0 Hz, 2H), 2.17–2.09 (m, 9H), 1.76–1.65 (m, 8H), 1.44–1.24 (m, 8H), 0.89 (t, *J* = 7.0 Hz, 3H). ^{13}C-NMR (126 MHz, $CDCl_3$) δ: 169.16, 149.25, 147.45, 147.28, 136.30, 133.26, 130.74, 125.92, 123.55, 123.48, 117.56, 112.05, 52.42, 43.19, 41.71, 36.37, 31.75, 29.49, 29.17, 29.06, 27.17, 22.60, 14.07. ESI-MS: m/s 468 $[M+Na]^+$.

***N*-(adamantan-1-yl)-2-(pentylamino)-5-(thien-2-yl)benzamide 12a.** Yield: 41%. mp: 142-143 °C. ^{1}H-NMR (500 MHz, $CDCl_3$) δ: 7.49 (dd, *J* = 9.0, 2.0 Hz, 1H), 7.45 (d, *J* = 2.0 Hz, 1H), 7.28 (s

546 br, 1H), 7.17 (dd, *J* = 4.5, 2.0 Hz 1H), 7.11 (dd, , *J* = 4.5, 2.0 Hz 1H), 7.28 (s br, 1H) 7.04–7.03 (m,
547 1H), 6.67 (d, *J* = 6.5 Hz, 1H), 5.73 (s br, 1H), 3.15 (q, *J* = 4.0 Hz, 2H) 2.17–2.06 (m, 9H), 1.76–1.64
548 (m, 8H), 1.41–1.33 (m, 4H), 0.92 (t, *J* = 7.0 *Hz*, 3H). ^{13}C-NMR (126 MHz, $CDCl_3$) δ: 169.12, 148.84,
549 144.66, 130.16, 127.85, 125.12, 122.94, 121.13, 121.02, 117.19, 111.73, 52.34, 43.20, 41.70, 36.38,
550 29.50, 29.39, 28.90, 22.48, 14.01.ESI-MS: m/z 421 $[M-H]^-$.

551 ***N*-(adamantan-1-yl)-2-(hexylamino)-5-(thien-2-yl)benzamide 12b.** Yield: 36%. mp: 97-98 °C.
552 ^{1}H-NMR (500 MHz, $CDCl_3$) δ: 7.50 (dd, *J* = 9.0, 2.0 Hz 1H), 7.46 (d, *J* = 2.0 Hz, 1H), 7.17 (dd, *J* =
553 4.5, 2.0 Hz, 1H), 7.12 (dd, *J* = 4.5, 2.0 Hz, 1H), 7.05–7.03 (m, 1H), 6.73 (d, *J* = 6.5 Hz, 1H), 5.75 (s
554 br, 1H), 3.15 (t, *J* = 7.5 Hz, 2H) 2.17–2.09 (m, 9H), 1.76–1.64 (m, 8H), 1.41 (quint, *J* = 7.5 Hz,
555 2H), 1.33–1.30 (m, 4H) 0.90 (t, *J* = 7.0 *Hz*, 3H). ^{13}C-NMR (126 MHz, $CDCl_3$) δ: 168.97, 148.29,
556 144.49, 130.17, 127.88, 125.06, 123.12, 121.32, 52.42, 41.68, 36.37, 31.57, 29.68, 29.49, 29.03,
557 26.86, 22.56, 14.01. ESI-MS: m/z = 459 $[M+Na]^+$.

558 ***N*-(adamantan-1-yl)-2-(heptylamino)-5-(thien-2-yl)benzamide 12c.** Yield: 42%. mp: 81-82 °C.
559 ^{1}H-NMR (500 MHz, $CDCl_3$) δ: 7.50 (dd, *J* = 9.0, 2.0 Hz, 1H), 7.46 (d, *J* = 2.0 Hz, 1H), 7.31 (s br,
560 1H), 7.17 (dd, *J* = 4.5, 2.0 Hz,1H), 7.12 (dd, *J*=4.5, 2.0 Hz 1H), 7.05–7.03 (m, 1H), 6.69 (d, *J* = 6.5
561 Hz, 1H), 5.74 (s br, 1H), 3.14 (t, *J* = 7.5 Hz, 2H), 2.17–2.09 (m, 9H), 1.76–1.64 (m, 8H), 1.43–1.28
562 (m, 8H) 0.89 (t, *J* = 7.0 Hz, 3H). ^{13}C-NMR (126 MHz, $CDCl_3$) δ: 169.07, 148.64, 144.60, 130.16,
563 129.15, 127.86, 125.10, 123.00, 121.20, 117.36, 111.95, 52.37, 43.39, 41.69, 36.38, 31.75, 29.50,
564 29.15, 29.06, 27.16, 22.60, 14.08. ESI-MS: m/z 473 $[M+Na]^+$.

565 ***N*-(adamantan-1-yl)-4'-fluoro-4-(pentylamino)-[1,1'-biphenyl]-3-carboxamide 13.** Yield:
566 55%. mp: 130-131°C. ^{1}H NMR (500 MHz, $CDCl_3$) δ: 7.46–7.42 (m, 3H), 7.40 (d, *J* = 2.0 Hz 1H),
567 7.22 (s br, 1H), 7.09 (t, *J* = 8.5 Hz 1H), 6.73 (d, *J* = 8.5 Hz 1H), 5.74 (s br, 1H), 3.16 (t, *J* = 7.0 Hz,
568 2H), 2.17–2.08 (m, 9H), 1.76–1.65 (m, 8H), 1.42–1.33 (m, 4H), 0.92 (t, *J* = 7.0 Hz 3H). ^{13}C-NMR
569 (126 MHz, $CDCl_3$) δ: 169.32, 162.77, 160.81, 137.00, 130.73, 127.70, 127.64, 125.77, 115.61,

115.44, 111.93, 52.34, 43.28, 41.73, 36.38, 29.49, 29.40, 28.91, 22.48, 14.02. ESI-MS: m/z 457 [M+Na]$^+$.

***N*-(adamantan-1-yl)-3'-fluoro-4-(pentylamino)-[1,1'-biphenyl]-3-carboxamide 14.** Yield: 48%. mp: 122-123 °C. ^{1}H NMR (500 MHz, $CDCl_3$) δ: 7.48 (dd, *J* = 9.0, 2.0 Hz, 1H), 7.44 (d, *J* = 2.0 Hz 1H), 7.37–7.33 (m, 1H), 7.31 (s br, 1H), 7.28 (dt, *J* = 9.0, 1.5 Hz, 1H), 7.19 (dt, *J* = 9.0, 1.5 Hz, 1H), 6.95 (m, 1H), 6.72 (d, *J* = 8.5, 1H), 5.75 (s br, 1H), 3.16 (q, *J* = 4.5 Hz, 2H), 2.17–2.08 (m, 9 H), 1.74–1.65 (m, 8H), 1.44–1.33(m, 4H), 0.93 (t, *J* = 7 Hz 3H), ^{13}C-NMR (126 MHz, $CDCl_3$) δ: 169.28, 164.24, 162.29, 149.09, 143.16, 130.74, 130.17, 125.86, 121.64, 117.35, 112.92, 112.75, 111.83, 52.37, 43.20, 41.72, 36.38, 29.50, 29.40, 28.91, 22.48, 14.02. ESI-MS: m/z 457 [M+Na]$^+$.

***N*-(adamantan-1-yl)-4'-methoxy-4-(pentylamino)-[1,1'-biphenyl]-3-carboxamide 15.** Yield: 42%. mp: 104-105°C. ^{1}H NMR (500 MHz, $CDCl_3$) δ: 7.56–7.12 (m, 1H), 7.43–7.42 (m, 1H), 7.42–7.42 (m, 2H), 6.97–6.95 (m, 3H), 6.79 (s br, 1H), 5.77 (sbr, 1H), 3.84 (s, 3H), 3.16, (t, *J* = 7.0 Hz 2H); 2.16–2.08 (m, 9H), 1.73–1.70 (m, 8H), 1.41–1.35 (m, 4H), 0.92 (t, *J* = 7.0 Hz 3H). ^{13}C-NMR (126 MHz, $CDCl_3$) δ: 130.63, 128.68, 128.12, 127.71, 127.33, 126.71, 126.62, 125.51, 114.23, 114.17, 114.14, 55.38, 55.33, 52.37, 41.71, 36.37, 29.49, 29.36, 28.78, 22.46, 14.01. ESI-MS: m/z 469 [M+Na]$^+$.

***N*-(adamantan-1-yl)-3'-methoxy-4-(pentylamino)-[1,1'-biphenyl]-3-carboxamide 16.** Yield: 52%. mp: 99-100 °C. ^{1}H NMR (500 MHz, $CDCl_3$) δ: 7.51–7.41 (m, 2H), 7.35–7.21 (m, 3H), 7.11-7.04 (m, 1H), 6.83 (dd, Hz, *J* = 8.0, 2.0 Hz, 1H), 6.72 (d, *J* = 8.0 Hz, 1H), 5.75 (s br, 1H), 3.86 (s, 3H), 3.20-3,07 (m, 2H), 2.21–1.98 (m, 9H), 1.77–1.63 (m, 8H), 1.41–1.35 (m, 4H), 0.92 (t, *J* = 7.0 Hz 3H), ^{13}C-NMR (126 MHz, $CDCl_3$) δ: 169.40, 159.95, 148.82, 142.42, 130.87, 129.72, 127.13, 125.96, 118.78, 117.31, 112.29, 111.77, 111.21, 55.31, 52.30, 43.24, 41.72, 36.39, 29.53, 29.41, 28.93, 22.49, 14.02. ESI-MS: m/z 469 [M+Na]$^+$.

***N*-((adamantan-1-yl)-4-(pentylamino)-[1,1'-biphenyl]-3,4'-dicarboxamide 17.** Yield: 40%. mp: 152-153 °C. ^{1}H NMR (500 MHz, $CDCl_3$) δ: 7.86 (d, *J* = 8.5 Hz, 2H), 7.59 (d, *J* = 8.5 Hz, 2H), 7.54 (dd, *J* = 8.5, 2.0 Hz, 1H), 7.50 (d, *J* = 2.0 Hz, 1H), 7.36 (s br, 1H) 6.75 (d, *J* = 8.5 Hz, 1H), 5.75 (s br,

1H), 3.17 (q, *J* = 6.0 Hz, 2H), 2.17–2.09 (m, 9H), 1.78–1.68 (m, 8H), 1.43–1.26 (m, 4H), 0.90 (t, *J* = 7 Hz 3H). ^{13}C-NMR (126 MHz, $CDCl_3$) δ: 169.24, 168.97, 151.90, 149.27, 144.43, 135.52, 130.85, 130.58, 127.95, 125.97, 117.47, 111.89, 52.41, 43.18, 41.71, 41.47, 36.37, 29.49, 28.87, 22.41, 14.01. ESI-MS m/z 482 $[M+Na]^+$.

***N*-((adamantan-1-yl)-4-(pentylamino)-[1,1'-biphenyl]-3,3'-dicarboxamide 18.** Yield: 40%. mp: 150-151 °C. ^{1}H NMR (500 MHz, $CDCl_3$) δ: 7.99 (t, *J* = 2.0 Hz, 1H), 7.66 (t, *J* = 8.0, 2.0 Hz, 1H), 7.53 (dd, *J* = 8.0, 2.0 Hz, 1H), 7.49–7.46 (m, 2H), 7.30 (s br, 1H), 6.73 (d, *J* = 8.0 Hz, 1H), 5,75 (s br, 1H), 3.18-3.15 (m, 2H), 2.16–2.10 (m, 9H), 1.79–1.65 (m, 8H), 1.44–1.34 (m, 4H), 0.94 (t, *J* = 7.0 Hz, 3H). ^{13}C-NMR (126 MHz, $CDCl_3$) δ: 169.27, 169.25, 149.06, 141.53, 133.79, 130.86, 129.71, 128.98, 126.05, 125.88, 125.34, 124.61, 117.50, 111.89, 52.42, 43.21, 41.69, 36.38, 29.50, 29.40, 28.90, 22.48, 14.02. ESI-MS m/z 482 $[M+Na]^+$.

Methyl 3'-((adamantan-1-yl)carbamoyl)-4'-(pentylamino)-[1,1'-biphenyl]-4-carboxylate 19. Yield: 58%. mp: 155-156°C. ^{1}H NMR (500 MHz, $CDCl_3$) δ: 8.19 (t, *J* = 1.5 Hz 1H), 7.93 (dt, , *J* = 7.5 1.5 Hz, 1H), 7.69 (dt, *J* = 7.5, 1.5 Hz, 1H), 7.53 (dd, , *J* = 9.0, 4.0 Hz, 1H), 7.49-7.40 (s br, 1H), 7.48 (d, *J* = 4.0 Hz 1H), 7.30 (t, *J* = 4.0 Hz 1H), 6.74 (d, *J* = 9.0 Hz 1H), 5.75 (s br, 1H), 3.95 (s, 3H), 3.16 (q, *J* = 5.5 Hz, 2H), 2.16–2.11 (m, 9H), 1.74–1.67 (m, 8H), 1.43–1.35 (m, 4H), 0.93 (t, *J* = 7.0 Hz 3H). ^{13}C-NMR (126 MHz, $CDCl_3$) δ: 169.29, 167.22, 149.01, 141.13, 130.86, 130.61, 130.56, 128.78, 127.18, 126.12, 125.85, 117.47, 111.89, 109.99, 52.39, 52.17, 43.21, 41.70, 36.39, 29.51, 29.40, 28.91, 22.48, 14.01. ESI-MS: m/z 497 $[M+Na]^+$.

***N*-(adamantan-1-yl)-4'-methyl-4-(pentylamino)-[1,1'-biphenyl]-3-carboxamide 20.** Yield: 33%. mp: 124-125 °C. ^{1}H NMR (300 MHz, $CDCl_3$) δ 7.48 (dd, *J* = 8.7, 2.3 Hz, 1H), 7.44 (d, *J* = 2.3 Hz, 1H), 7.42 – 7.37 (m, 2H), 7.21 (d, *J* = 7.8 Hz, 2H), 6.72 (d, *J* = 8.7 Hz, 1H), 5.74 (s br, 1H), 3.15 (q, *J* = 4.5 Hz, 2H), 2.38 (s, 3H), 2.15-2.08 (m, 9H), 1.76 – 1.66 (m, 8H), 1.42-1.38 (m, 4H), 0.92 (t, *J* = 7.2 Hz, 3H). ^{13}C-NMR (126 MHz, $CDCl_3$) δ 169.43, 138.00, 135.94, 130.74, 129.44, 126.10, 125.76, 52.28, 41.72, 36.39, 29.50, 29.41, 28.92, 22.49, 21.02, 14.03. ESI-MS m/z 453 $[M+Na]^+$.

***N*-(adamantan-1-yl)-3'-methyl-4-(pentylamino)-[1,1'-biphenyl]-3-carboxamide 21.** Yield: 35%. mp: 109-110°C. ^{1}H NMR (300 MHz, $CDCl_3$) δ 7.49 (dd, *J* = 8.7, 2.1 Hz, 1H), 7.44 (d, *J* = 2.1 Hz, 1H), 7.30 (d, *J* = 5.0 Hz, 3H), 7.10 (t, *J* = 5.0 Hz, 1H), 6.72 (d, *J* = 8.7 Hz, 1H), 5.75 (s br, 1H), 3.16 (q, *J* = 4.5 Hz, 2H), 2.41 (s, 3H), 2.17-2.07 (m, 9H), 1.75 – 1.66 (m, 8H), 1.43 – 1.35 (m, 4H), 0.92 (t, *J* = 7.0 Hz, 3H). ^{13}C-NMR (126 MHz, $CDCl_3$) δ 169.42, 140.85, 138.34, 130.93, 128.66, 127.03, 125.93, 123.38, 52.31, 41.72, 36.39, 29.68, 29.50, 29.41, 28.91, 22.49, 21.56, 14.02. ESI-MS m/z 453 $[M+Na]^+$.

Synthesis Methyl 4-amino-[1,1'-biphenyl]-3-carboxylate 22. The commercial available methyl 2-aminobenzoate (1.00g, 4.4 mmol) and the phenylboronic acid (6.5 mmol 0,80g) were suspended in a solution of dioxane (24.0 mL) and K_2CO_3 2M (6.0 ml). N_2 was bubbled in the solution, for 10 minutes. Then, $Pd(PPh_3)_4$ (0.50g, 0.44 mmol) is added and the solution was heated at reflux for about 2 hours. The solvent was removed under reduced pressure and the resulting residue was purified by a flash column chromatography (eluent: n-hexane/ ethyl acetate 9.5/0.5 to 9/1) obtaining compound **22**. Yield: 50%. ^{1}H NMR (300 MHz, $CDCl_3$) δ: 8.12 (s, 1H), 7.56–7.53 (m, 3H), 7.40 (t, *J* = 9.0 Hz, 2H), 7.29 (d, *J* = 7.51 Hz, 1H), 6.75 (d, *J* = 6.0 Hz, 1H), 5.78 (sbr, 2H), 3.90 (s, 3H). ESI-MS m/z: 250 $[M+Na]^+$.

Synthesis of methyl 4-(pentylamino)-[1,1'-biphenyl]-3-carboxylate 23. In a reaction flask which was dried under argon, the intermediate **22** (0.40 g, 1.8 mmol) was suspended in anhydrous THF (20 ml). Pentanal (0.6 mL, 5.4 mmol) was added and the mixture was left under magnetic stirring for 3 hour at room temperature. The $NaBH(OAc)_3$ (0.76 g, 3.6 mmol) was added at 0 °C to the mixture and the solution was left under magnetic stirring overnight at room temperature. After the addition of methanol (10.0 ml) the solvent was removed under reduced pressure. The resulting residue was purified by flash gradient column chromatography (eluent: n-hexane/ ethyl acetate: 9.5/0.5 to 9 /1) to obtain compound **23**. Yield: 79%. ^{1}H NMR (500 MHz, $CDCl_3$) δ: 8.19 (d, *J* = 2.0 Hz, 1H), 7.76 (s br, 1H), 7.63 (dd, *J* = 8.0, 2.0 Hz, 1H), 7.56 (dd, *J*= 8.0, 2.0 Hz , 2H), 7.41 (t, *J* = 8.0 Hz, 2H), 7.27

(t, J = 8.0 Hz 1H), 6.76 (d, J = 8.0 Hz, 1H), 3.89 (s, 3H), 3.23 (q, J = 6.5 Hz, 2H), 1.72 (quint, J = 6.5 Hz, 2H), 1.47–1.39 (m, 4H), 0.95 (t, J = 7.0 Hz, 3H). ESI-MS: m/z 280 $[M+Na]^+$.

4-(pentylamino)-[1,1'-biphenyl]-3-carboxylic acid 24. Intermediate **23** (0.23 g, 0.8 mmol) is dissolved in a 1:1 solution of NaOH (2N) (6.3 mL) and EtOH absolute (6.3 mL). The reaction mixture is left under magnetic stirring at room temperature for 4 hours. The solution is then acidified with HCl (3N) until a precipitate is formed (pH = 4/5). The product is recovered by filtration, washing with water at pH = 4/5 and dried under vacuum obtaining the corresponding carboxylic acid **24**. Yield: 43%. ^{1}H NMR (300 MHz, $CDCl_3$) δ: 8.21 (d, J = 2.0 Hz, 1H), 7.63 (dd, J = 7.5, 2.0 Hz, 1H), 7.57-7.51 (m, 2H), 7.37 (t, J = 7.5 Hz, 2H), 7.28, 7.20 (m, 2H), 6.6 (d, J = 7.5 Hz, 1H), 3.21 (t, J = 7.0 Hz, 2H), 1.60 (quint, J = 7.0 Hz, 2H), 1.45–1.29 (m, 4H), 0.91 (t, J = 7.0 Hz, 3H). ESI-MS: m/z 282 $[M-H]^-$.

***N*-cyclohexyl-4-(pentylamino)-[1,1'-biphenyl]-3-carboxamide 25.** Intermediate **24** (0.03 g, 0.11 mmol) was placed in a reaction flask, previously dried under argon, and dissolved in anhydrous DMF (0.5 mL). DIPEA (0.06 mL) is added at 0 °C, and the mixture is left under magnetic stirring at 0 °C for 10 minutes in argon current. HBTU (0.062 g, 0.165 mmol) is added to the solution and the mixture is left at room temperature for 2 hours. Cyclohexylamine (0.033 g, 0.33 mmol) is added to the solution. The system is left under magnetic stirring overnight at room temperature and the solvent was removed under reduced pressure. The resulting crude was purified by flash gradient column chromatography (n-hexane/ ethyl acetate: 9.5/0.5 to 9/1) obtaining the final compound **25** Yield: 74%. mp: 113-114°C. ^{1}H NMR (500 MHz, $CDCl_3$) δ: 7.55–7.50 (m, 4H), 7.45–7.40 (m, 2H), 7.30–7.25 (m, 1H), 6.80 (d, J = 7.5 Hz, 1H), 6.01 (s br, 1H), 3.99–3.90 (m, 1H), 3.18 (t, J = 7.0 Hz, 2H), 2.05-2.02 (m, 2H), 1.78–1.65 (m, 6H), 1.43–1.37 (m, 4H), 1.28–1.18 (m, 4H), 0.92 (t, J = 7.0 Hz 3H). ^{13}C-NMR (126 MHz, $CDCl_3$) δ: 168.86, 140.71, 131.29, 129.55, 128.77, 126.37, 126.26, 125.77, 120.42, 115.32, 48.49, 43.69, 33.25, 29.38, 28.79, 25.57, 24.97, 22.47, 13.99. ESI-MS: m/z 387 $[M+Na]^+$.

Biological Evaluation. Materials. Cell culture reagents were purchased from Celbio s.r.l. (Milano, Italy) and culturePlate 96/wells plates from PerkinElmer Life Science; GW405833 and (R)-(þ)-WIN

55,212-2 were purchased from TOCRIS (Milan, Italy) and Multiscreen HTS filter plates from Merck Millipore (Ireland). OptiPhase Supermix and [3H] -CP55940 were purchased from PerkinElmer Life Science.

Cell cultures. CB2R-HEK293 and CB1R-HEK293 cells were grown in DMEM high glucose supplemented with 10% fetal bovine serum, 2 mM glutamine,100 U/mL penicillin,100 mg/mL streptomycin, 0.1 mg/mL G418, in a humidified incubator at 37 °C with a 5% CO2 atmosphere. Human monocyte THP-1 cells, obtained from ATCC (Manassas, VA) were seeded at 1 x 10^5 cells/ml for 48 h. To differentiate cells into macrophages, 0.01 µM PMA was added for 48 h. By microscope analysis, in these conditions 98% cells became adherent. To stimulate THP-1 monocytes and adherent cells, 10 µg/ml of LPS was added for 24 h, as reported in Dreskin, 2001. Cells were cultured in RPMI-1640 medium supplemented with 10% fetal bovine serum, 2 mM glutamine,100 U/mL penicillin,100 mg/mL streptomycin, in a humidified incubator at 37 °C with a 5% CO_2 atmosphere.[84]

Radioligand binding assay. Membrane preparations for CB1R and CB2R ~~receptors~~ assays. CB1R-HEK293 cells membranes were prepared by scratching the cells off the previously frozen cell culture dishes in Phosphate Buffered Saline (PBS, pH 7.4). The cell suspension was centrifuged at 800xg for 15 min and the pellet resuspended and homogenized on ice for 1 min by a dounce homogenizer, and subsequently spun down for 5 min at 4 °C and 500 g. The supernatant was centrifuged for 20 min at 25,000 g and the obtained membrane pellets resuspended in buffer A (10 mM $NaHCO_3$, 10 mM EGTA, 10 mM EDTA, 1X protease inhibitors cocktail, pH = 7.4), centrifuged for 20 min at 25,000 g and the pellet resuspended in the required amount of 25 mM Tris-HCl buffer, 5 mM $MgCl_2$, 1 mM EDTA, pH 7.4. Aliquots of the membrane preparation were stored at -80°C until being used.[29]

CB2R-HEK293 cells membranes were prepared by scratching the cells off the previously frozen cell culture dishes in ice-cold hypotonic buffer (5 mM Tris-HCl, 2 mM EDTA, pH 7.4). The cell suspension, firstly homogenized on ice for 1 min by an Ultra-Turrax (T25basic, IKALABORTECHNIK, Higashiosaka, Japan), was further homogenized for 1 min with a dounce

698 homogenizer, and subsequently spun down for 10 min at 4 °C and 1000 g. The supernatant centrifuged
699 for 60 min at 48,000 and the obtained pellets resuspended and homogenized in the required amount
700 of 50 mM Tris-HCl buffer, pH 7.4. Aliquots of the membrane preparation were stored at -80 °C until
701 use.[29]

702 **CB2R and CB1R Radioligand competition binding assays.** Competition binding assays were
703 performed as reported in Spinelli et al.[29] CB2R-HEK293 membranes (50 µg protein/well) were used
704 as human CB2R ~~receptor~~ source and the CB agonist [3H](-)-cis-3-[2-hydroxy-4-(1,1-
705 dimethylheptyl) phenyl]-trans-4-(3-hydroxypropyl)cyclohexanol (CP55,940), (PerkinElmer Italia
706 SPA, Milano, Italy) as radioligand. After addition of 25 µL of the test compounds at different
707 concentrations (10^{-12}-10^{-5}M), 25 µL of [3H]CP55,940 solution in assay buffer (at final concentration
708 of 0.2 nM), and 100 µL of membrane preparation to 100 µL of assay buffer (50Mm Tris, 2,5mM
709 EGTA, 5mM MgCl2, 0.1% fatty acid fere bovine serum albumine BSA, pH 7.4), the suspension was
710 incubated for 90 min at 30 °C. Total binding was determined without the test compounds. Nonspecific
711 binding was determined in the presence of 10 µM GW405833, CB2R reference compound. The
712 incubation was stopped by rapid filtration through a GF/C glass fibre filter (Merck Millipore, Ireland)
713 presoaked for 30 min with 0.05% aq. Polyethyleneimine solution, using a 96-channel cell harvester
714 (Merck Millipore, Ireland). The filter was washed three times with 100 µL ice-cold washing buffer
715 (50 mM Tris, 2,5 mM EGTA, 5 mM $MgCl_2$, 1% BSA, pH 7.4),) and then dried for 1.5 h at 50 °C.
716 Radioactivity on the filter was determined in a MicroBeta JET counter (Perkin- Elmer, Boston, MA,
717 USA) after 6 h of preincubation with 100 µl of scintillation cocktail (OptiPhase superMix, Perkin-
718 Elmer). Data were obtained in three independent experiments, performed in triplicates. Data were
719 analyzed using GraphPad Prism Version 7 (San Diego, CA, USA). For the calculation of K_i values,
720 the Cheng-Prusoff equation and a K_d value of 1.5 nM ([3H]CP55,940 at CB2) were used.

721 ~~Cannabinoid~~ CB1R ~~receptor~~ competition binding experiments were carried out in a polypropilene
722 well 20 µg of membranes from HEK 293-hCB1 cell line, 0.8 nM [3H]-CP55940 (164.9 Ci/mmol, 1

mCi/mL, Perkin Elmer NET1051250UC) and studied and standard compounds were incubated. Non-specific binding was determined in the presence of Surinabant 10 μM. The reaction mixture was incubated at 30 °C for 60 min, 200 μL were trasnfered to GF/C 96-well plate (Millipore, Madrid, Spain) pretreated with binding buffer (Tris-HCl 50 mM, EDTA 1 mM, $MgCl_2$ 5 mM, BSA 0.5%, pH ¼ 7.4), after was filtered and washed four times with 250 μL wash buffer (Tris-HCl 50 mM, EDTA 1 mM, $MgCl_2$ 5 mM, BSA 0.5%, pH ¼ 7.4), before measuring in a microplate beta scintillation counter (Microbeta Trilux, PerkinElmer, Madrid, Spain). Data were obtained in three independent experiments, performed in triplicates.

Functional Activity at CB2R In Vitro. Gi-coupled cAMP modulation was measured following the manufacturer's protocol (Eurofins, Fremont, CA) as previously reported.[85] Briefly, CHO-K1 cells overexpressing the human CB2R were plated into a 96-well plate (30 000 cells/well) and incubated overnight at 37 °C, 5% CO_2. Media was aspirated and replaced with 30 μL of assay buffer. Cells were incubated for 30 min at 37 °C with 15 μL of 3× dose−response solutions of samples prepared in the presence of a cell assay buffer containing 3× of 25 μM NKH-477 solution to stimulate adenylate cyclase and enhance basal cAMP levels. For those compounds showing an increase of cAMP levels, we further investigated their effect upon receptor activation by testing compounds in the presence of the JWH-133 selective agonist. Cells were pre-incubated with samples (15 min at 37 °C at 6× the final desired concentration) followed by 30 min incubation with the JWH-133 agonist challenge at the EC80 concentration (EC80 = 4 μM, previously determined in separate experiments) in the presence of NKH-477 to stimulate adenylate cyclase and enhance cAMP levels. For all protocols, following stimulation, cell lysis and cAMP detection were performed as per the manufacturer's protocol. Luminescence measurements were performed using a GloMax Multi Detection System (Promega, Italy). Data are reported as means ± SEM of three independent experiments conducted in triplicate and were normalized considering the NKH-477 stimulus alone as 100% of the response. Data were analyzed using PRISM.9.3 software (GraphPad Software Inc, San Diego, CA).[85]

Anti-inflammatory and pro-inflammatory cytochine detection. The amount of cytokines was measured in 5 µL of supernatants, derived from 1 x 10^4 cells, using the ProQuantum immunoassays kits fro TNF-α, IFN-γ, IL-1β, IL-6, IL-10, IL-4, IL-17A (ThermoFisher Scientific, Waltham, MA), according to the manufacturer's instructions. The results were expressed as pg/ml based on the titration curved of each kits.

Molecular docking simulations. Compounds **4** and **10a** were docked on the recently published x-ray structures of CB2R in complex with the antagonist AM10257 (PDB code: 5ZTY - resolution: 2.80 Å)[71] and the agonist AM12033 (PDB code: 6KPC - resolution: 3.20 Å).[4] The retrieved .pdb files were pre-treated using the Protein Preparation Wizard (PPW) tool available from the Schrödinger suite.[86] Such a tool allows adding missing hydrogen atoms, reconstructing incomplete side chains, assigning the ionization states at physiological pH, setting the orientation of any misoriented groups, removing water molecules, and optimizing the hydrogen bond network. Finally, using the OPLS4 force field,[87] a restrained minimization was performed. In both cases, a cubic grid was generated on the centroid of the cognate ligand. In doing that, we obtained an inner box of 10 Å × 10 Å × 10 Å irrespective of the considered protein structure, and an outer box of 25 Å × 25 Å × 25 Å (26 Å × 26 Å × 26 Å) in 5ZTY (6KPC). Both the ligands, **4** and **10a**, were subjected to LigPrep[88]a tool available from the Schrodinger Suite 2021-4, to build the 3D structures retaining the correct chirality specified in each SMILE string, desalt and generate all the tautomers and ionization states at a pH value of 7.0 ± 2.0. All docking simulations were performed using the default force field OPLS_2005[89] and the extra precision docking (XP) protocol with an expanded sampling, keeping the protein fixed and allowing conformational flexibility for the ligands. Importantly, such a protocol was validated by redocking the cognate ligands (RMSD = 0.55 Å for AM10257; RMSD = 0.71 Å for AM12033).

MM-GBSA calculations. Following a protocol published elsewhere,[90] we applied the molecular mechanics/generalized Born surface area approach (MM-GBSA);[91] to the obtained top-scored docking poses to compute the binding free energies (ΔG) between protein and ligands. During this

calculation, flexibility was allowed for all residues having at least one atom within a distance of 5 Å from the ligand.

ASSOCIATED CONTENT

Supplementary material

Representative Spectra ^{1}H and ^{13}C and HPLC analysis for compounds **4** and **10a**~~,~~ ~~and~~ HPLC purity analyses data of *N*-adamantyl-anthranil amides **4–21**, ~~and~~ **25** and in vitro biological evaluation of the CB2R activity profile **11a**, **12a** and **14** are available free of charge.

AUTHOR INFORMATION

Corresponding Author

* Angela Stefanachi − Dipartimento di Farmacia-Scienze del Farmaco, Università degli Studi di Bari Aldo Moro, 70125 Bari, Italy; orcid.org/0000-0002-9430-7972; Phone: +0390805442783; Email: angela.stefanachi@uniba.it

* Marialessandra Contino − Dipartimento di Farmacia-Scienze del Farmaco, Università degli Studi di Bari Aldo Moro, 70125 Bari, Italy; orcid.org/0000-0002-0713-3151; Phone: +0390805442751; Email: marialessandra.contino@uniba.it

Author

Giovanni Graziano−Dipartimento di Farmacia-Scienze del Farmaco, Università degli Studi di Bari Aldo Moro, 70125 Bari, Italy; https://orcid.org/0000-0002-5575-3240;

Pietro Delre−Institute of Crystallography, National Research Council of Italy, Via Amendola, 122/o, 70126 Bari;

Francesca Carofiglio−Dipartimento di Farmacia-Scienze del Farmaco, Università degli Studi di Bari Aldo Moro, 70125 Bari, Italy;

Codice campo modificato

Codice campo modificato

Jose Brea-Innopharma Screening Platform, BioFarma Research Group, Center for Research in Molecular Medicine and Chronic Diseases (CIMUS), University of Santiago de Compostela, Santiago de Compostela, Spain; Department of Pharmacology, Pharmacy and Pharmaceutical Technology. School of Pharmacy. University of Santiago de Compostela, Santiago de Compostela, Spain;

Alessia Ligresti- Institute of Biomolecular Chemistry, National Research Council of Italy, Via Campi Flegrei 34, 80078 Pozzuoli (Na), Italy;

Magdalena Kostrzewa- cInstitute of Biomolecular Chemistry, National Research Council of Italy, Via Campi Flegrei 34, 80078 Pozzuoli (Na), Italy;

Chiara Riganti-Dipartimento di Oncologia, Università degli Studi di Torino, Torino, Italy;

Claudia Gioè-Gallo- ComBioMed Research Group, Centro de Química Biológica y Materiales Moleculares (CIQUS) University of Santiago de Compostela, Santiago de Compostela, Spain;

Maria Majellaro- ComBioMed Research Group, Centro de Química Biológica y Materiales Moleculares (CIQUS) University of Santiago de Compostela, Santiago de Compostela, Spain;

Orazio Nicolotti- Dipartimento di Farmacia-Scienze del Farmaco, Universita degli Studi di Bari ALDO MORO, via Orabona 4, 70125, Bari, Italy;

Nicola Antonio Colabufo- Dipartimento di Farmacia-Scienze del Farmaco, Universita degli Studi di Bari ALDO MORO, via Orabona 4, 70125, Bari, Italy;

Carmen Abate - Dipartimento di Farmacia-Scienze del Farmaco, Universita degli Studi di Bari ALDO MORO, via Orabona 4, 70125, Bari, Italy; bInstitute of Crystallography, National Research Council of Italy, Via Amendola, 122/o, 70126 Bari; https://orcid.org/0000-0001-9292-884X

Maria Isabel Loza- Innopharma Screening Platform, BioFarma Research Group, Center for Research in Molecular Medicine and Chronic Diseases (CIMUS), University of Santiago de Compostela, Santiago de Compostela, Spain;e Department of Pharmacology, Pharmacy and Pharmaceutical Technology. School of Pharmacy. University of Santiago de Compostela, Santiago de Compostela, Spain;

Eddy Sotelo Perez- ComBioMed Research Group, Centro de Química Biológica y Materiales Moleculares (CIQUS) University of Santiago de Compostela, Santiago de Compostela, Spain;
Giuseppe Felice Mangiatordi- Institute of Crystallography, National Research Council of Italy, Via Amendola, 122/o, 70126 Bari;
Francesco Leonetti- Dipartimento di Farmacia-Scienze del Farmaco, Università degli Studi di Bari ALDO MORO, via Orabona 4, 70125, Bari, Italy.

Author Contributions

The manuscript was written through contributions of all authors. All authors have given approval to the final version of the manuscript. # G.G. and P.D. contributed equally.

Funding Sources

ML and JB acknowledged the funding from Agencia Estatal de Investigación (PID2020-119428RB-I00) and Xunta de Galicia (ED431C 2018/21 and ED431G 2019/02) and European Regional Development Fund (ERDF) in the frame of the Recovery Assistance for Cohesion and the Territories of Europe (REACT-EU) funds
ES acknowledged financial support by the Consellería de Cultura, Educación e Ordenación Universitaria of the Galician Government: (grant: ED431B 2020/43), Centro Singular de Investigación de Galicia accreditation 2019-2022 (ED431G 2019/03).

Notes

The authors declare no competing financial interest.

ACKNOWLEDGMENT

We acknowledge Rocio Piña Márquez for the technical support on binding experiments. MC thanks EMBO fellowship ST8165 for fruitful scientific link with the CIMUS Institute. GG, ES, MC and AS

gratefully thanks COST Action 18133 ERNEST for networking. GG, gratefully thanks A.Re.S.S.puglia for dissemination support.

ABBREVIATIONS

CB2R, cannabinoid receptor type 2; CB1R, cannabinoid receptor type 1; ECS, endocannabinoid system; CNS, central nervous system; *K*i, inhibitor constant; TRPV-1, receptor potential vanilloid type 1; GPR, G protein-coupled receptor; Δ^9-THC, Δ^9-tetrahydrocannabinol; COVID-19, Coronavirus disease 2019; LPS, lipopolysaccharide; DIPEA, *N,N*-diisopropylethylamine; DMF, dimethylformamide; HBTU, 3-[Bis(dimethylamino)methyliumyl]-3H-benzotriazol-1-oxide hexafluorophosphate; THF, tetrahydrofuran; DCM, dichloromethane; Rt, room temperature; cAMP, cyclic adenosine monophosphate; nM, nanomolar; µM, micromolar; PDB, code protein data bank; MM-GBSA, Molecular mechanics with generalised Born and surface area solvation; NKH-477, colforsin dapropate hydrochloride; EC_{50}, maximal effective concentration; NAFLD, non-alcoholic fatty liver disease; TNF-α, tumor necrosis factor α, IFN-γ, interferon gamma; IL1-β ,interleukin 1 beta; IL-6, interleukin 6; IL-4, interleukin 4; IL-10, interleukin 10; LPS, lipopolysaccharides; THP-1, human monocytic cell line derived from an acute monocytic leukemia patient; ELISA, enzyme-linked immunosorbent assay; qRT-PCR, real-time polymerase chain reaction; SEM, standard error of mean; ANOVA, analysis of variance; TLC, thin layer chromatography, DMSO-d_6 , deuterated dimethyl sulfoxide; CDCl3, deuterated chloroform; MHz, megahertz; Hz, hertz; Ppm, parts per million; HPLC, high performance liquid chromatography; DAD, diode-array detector; NMR, nuclear magnetic resonance; J, coupling constant; mmol, millimole; µL, microliter; PBS, phosphate buffered saline; DMEM, Dulbecco's modified eagle medium; PMA, phorbol 12-myristate 13-acetate; EDTA, ethylenediaminetetraacetic acid; BSA, bovine serum albumin; PPW, protein preparation wizard;

SMILE, simplified molecular input line entry specification; RMSD, root-mean-square deviation of atomic positions.

REFERENCES

(1) Han, S.; Thatte, J.; Buzard, D. J.; Jones, R. M. Therapeutic Utility of Cannabinoid Receptor Type 2 (CB(2)) Selective Agonists. *J Med Chem* **2013**, *56* (21), 8224–8256. https://doi.org/10.1021/jm4005626.

(2) Pacher, P.; Kunos, G. Modulating the Endocannabinoid System in Human Health and Disease: Successes and Failures. *FEBS J* **2013**, *280* (9), 1918–1943. https://doi.org/10.1111/febs.12260.

(3) Di Marzo, V.; Bifulco, M.; De Petrocellis, L. The Endocannabinoid System and Its Therapeutic Exploitation. *Nat Rev Drug Discov* **2004**, *3* (9), 771–784. https://doi.org/10.1038/nrd1495.

(4) Hua, T.; Li, X.; Wu, L.; Iliopoulos-Tsoutsouvas, C.; Wang, Y.; Wu, M.; Shen, L.; Brust, C. A.; Nikas, S. P.; Song, F.; Song, X.; Yuan, S.; Sun, Q.; Wu, Y.; Jiang, S.; Grim, T. W.; Benchama, O.; Stahl, E. L.; Zvonok, N.; Zhao, S.; Bohn, L. M.; Makriyannis, A.; Liu, Z.-J. Activation and Signaling Mechanism Revealed by Cannabinoid Receptor-Gi Complex Structures. *Cell* **2020**, *180* (4), 655-665.e18. https://doi.org/10.1016/j.cell.2020.01.008.

(5) Piomelli, D. The Molecular Logic of Endocannabinoid Signalling. *Nat Rev Neurosci* **2003**, *4* (11), 873–884. https://doi.org/10.1038/nrn1247.

(6) Howlett, A. C. Cannabinoid Receptor Signaling. *Cannabinoids* **2005**, 53–79.

(7) Matsuda, L. A.; Lolait, S. J.; Brownstein, M. J.; Young, A. C.; Bonner, T. I. Structure of a Cannabinoid Receptor and Functional Expression of the Cloned CDNA. *Nature* **1990**, *346* (6284), 561–564.

(8) Pertwee, R. G.; Howlett, A. C.; Abood, M. E.; Alexander, S. P. H.; Marzo, V. D.; Elphick, M. R.; Greasley, P. J.; Hansen, H. S.; Kunos, G.; Mackie, K.; Mechoulam, R.; Ross, R. A. International Union of Basic and Clinical Pharmacology. LXXIX. Cannabinoid Receptors and Their Ligands: Beyond CB1 and CB2. *Pharmacol Rev* **2010**, *62* (4), 588–631. https://doi.org/10.1124/pr.110.003004.

(9) Munro, S.; Thomas, K. L.; Abu-Shaar, M. Molecular Characterization of a Peripheral Receptor for Cannabinoids. *Nature* **1993**, *365* (6441), 61–65. https://doi.org/10.1038/365061a0.

(10) Contino, M.; McCormick, P. J. Editorial: The Canonical and Non-Canonical Endocannabinoid System as a Target in Cancer and Acute and Chronic Pain. *Frontiers in Pharmacology* **2020**, *11*.

(11) Pacher, P.; Bátkai, S.; Kunos, G. The Endocannabinoid System as an Emerging Target of Pharmacotherapy. *Pharmacol Rev* **2006**, *58* (3), 389–462. https://doi.org/10.1124/pr.58.3.2.

(12) Pertwee, R. G. Emerging Strategies for Exploiting Cannabinoid Receptor Agonists as Medicines. *British Journal of Pharmacology* **2009**, *156* (3), 397–411. https://doi.org/10.1111/j.1476-5381.2008.00048.x.

(13) Pertwee, R. G. Targeting the Endocannabinoid System with Cannabinoid Receptor Agonists: Pharmacological Strategies and Therapeutic Possibilities. *Philosophical Transactions of the Royal Society B: Biological Sciences* **2012**, *367* (1607), 3353–3363. https://doi.org/10.1098/rstb.2011.0381.

(14) Ameri, A. The Effects of Cannabinoids on the Brain. *Progress in Neurobiology* **1999**, *58* (4), 315–348. https://doi.org/10.1016/S0301-0082(98)00087-2.

(15) Farquhar-Smith, W. P.; Egertová, M.; Bradbury, E. J.; McMahon, S. B.; Rice, A. S. C.; Elphick, M. R. Cannabinoid CB1 Receptor Expression in Rat Spinal Cord. *Molecular and Cellular Neuroscience* **2000**, *15* (6), 510–521. https://doi.org/10.1006/mcne.2000.0844.
(16) Gaoni, Y.; Mechoulam, R. *Isolation, Structure, and Partial Synthesis of an Active Constituent of Hashish*. ACS Publications. https://doi.org/10.1021/ja01062a046.
(17) Mechoulam, R.; Burstein, S. H. *Marijuana; Chemistry, Pharmacology, Metabolism and Clinical Effects.*; Academic Press: New York, 1973.
(18) Das, S. K.; Paria, B. C.; Chakraborty, I.; Dey, S. K. Cannabinoid Ligand-Receptor Signaling in the Mouse Uterus. *Proceedings of the National Academy of Sciences* **1995**, *92* (10), 4332–4336. https://doi.org/10.1073/pnas.92.10.4332.
(19) Galiègue, S.; Mary, S.; Marchand, J.; Dussossoy, D.; Carrière, D.; Carayon, P.; Bouaboula, M.; Shire, D.; LE Fur, G.; Casellas, P. Expression of Central and Peripheral Cannabinoid Receptors in Human Immune Tissues and Leukocyte Subpopulations. *European Journal of Biochemistry* **1995**, *232* (1), 54–61. https://doi.org/10.1111/j.1432-1033.1995.tb20780.x.
(20) Wenger, T.; Ledent, C.; Csernus, V.; Gerendai, I. The Central Cannabinoid Receptor Inactivation Suppresses Endocrine Reproductive Functions. *Biochemical and Biophysical Research Communications* **2001**, *284* (2), 363–368. https://doi.org/10.1006/bbrc.2001.4977.
(21) Gérard, C. M.; Mollereau, C.; Vassart, G.; Parmentier, M. Molecular Cloning of a Human Cannabinoid Receptor Which Is Also Expressed in Testis. *Biochemical Journal* **1991**, *279* (1), 129–134. https://doi.org/10.1042/bj2790129.
(22) Atwood, B. K.; Mackie, K. CB2: A Cannabinoid Receptor with an Identity Crisis. *British Journal of Pharmacology* **2010**, *160* (3), 467–479. https://doi.org/10.1111/j.1476-5381.2010.00729.x.
(23) Yao, B.; Mackie, K. Endocannabinoid Receptor Pharmacology. In *Behavioral Neurobiology of the Endocannabinoid System*; Kendall, D., Alexander, S., Eds.; Current Topics in Behavioral Neurosciences; Springer: Berlin, Heidelberg, 2009; pp 37–63. https://doi.org/10.1007/978-3-540-88955-7_2.
(24) Cabral, G. A.; Raborn, E. S.; Griffin, L.; Dennis, J.; Marciano-Cabral, F. CB2 Receptors in the Brain: Role in Central Immune Function. *British Journal of Pharmacology* **2008**, *153* (2), 240–251. https://doi.org/10.1038/sj.bjp.0707584.
(25) Onaivi, E. S.; Ishiguro, H.; Gong, J.-P.; Pa^{TEL}, S.; Perchuk, A.; Meozzi, P. A.; Myers, L.; Mora, Z.; Tagliaferro, P.; Gardner, E.; Brusco, A.; Akinshola, B. E.; Liu, Q.-R.; Hope, B.; Iwasaki, S.; Arinami, T.; Teasenfitz, L.; Uhl, G. R. Discovery of the Presence and Functional Expression of Cannabinoid CB2 Receptors in Brain. *Annals of the New York Academy of Sciences* **2006**, *1074* (1), 514–536. https://doi.org/10.1196/annals.1369.052.
(26) Stempel, A. V.; Stumpf, A.; Zhang, H.-Y.; Özdoğan, T.; Pannasch, U.; Theis, A.-K.; Otte, D.-M.; Wojtalla, A.; Rácz, I.; Ponomarenko, A.; Xi, Z.-X.; Zimmer, A.; Schmitz, D. Cannabinoid Type 2 Receptors Mediate a Cell Type-Specific Plasticity in the Hippocampus. *Neuron* **2016**, *90* (4), 795–809. https://doi.org/10.1016/j.neuron.2016.03.034.
(27) Maccarrone, M.; Bab, I.; Bíró, T.; Cabral, G. A.; Dey, S. K.; Di Marzo, V.; Konje, J. C.; Kunos, G.; Mechoulam, R.; Pacher, P.; Sharkey, K. A.; Zimmer, A. Endocannabinoid Signaling at the Periphery: 50 Years after THC. *Trends in Pharmacological Sciences* **2015**, *36* (5), 277–296. https://doi.org/10.1016/j.tips.2015.02.008.
(28) Whiting, Z. M.; Yin, J.; Sara, M.; Vernall, A. J.; Grimsey, N. L. Developing the Cannabinoid Receptor 2 (CB2) Pharmacopoeia: Past, Present, and Future. *Trends in Pharmacological Sciences* **2022**.
(29) Spinelli, F.; Capparelli, E.; Abate, C.; Colabufo, N. A.; Contino, M. Perspectives of Cannabinoid Type 2 Receptor (CB2R) Ligands in Neurodegenerative Disorders: Structure–Affinity Relationship (SAfiR) and Structure–Activity Relationship (SAR) Studies. *J. Med. Chem.* **2017**, *60* (24), 9913–9931. https://doi.org/10.1021/acs.jmedchem.7b00155.

(30) Benito, C.; Tolón, R. M.; Pazos, M. R.; Núñez, E.; Castillo, A. I.; Romero, J. Cannabinoid CB2 Receptors in Human Brain Inflammation. *British Journal of Pharmacology* **2008**, *153* (2), 277–285. https://doi.org/10.1038/sj.bjp.0707505.
(31) Boche, D.; Perry, V. H.; Nicoll, J. a. R. Review: Activation Patterns of Microglia and Their Identification in the Human Brain. *Neuropathology and Applied Neurobiology* **2013**, *39* (1), 3–18. https://doi.org/10.1111/nan.12011.
(32) Vitale, R. M.; Iannotti, F. A.; Amodeo, P. The (Poly)Pharmacology of Cannabidiol in Neurological and Neuropsychiatric Disorders: Molecular Mechanisms and Targets. *International Journal of Molecular Sciences* **2021**, *22* (9), 4876. https://doi.org/10.3390/ijms22094876.
(33) Contino, M.; Capparelli, E.; Colabufo, N. A.; Bush, A. I. Editorial: The CB2 Cannabinoid System: A New Strategy in Neurodegenerative Disorder and Neuroinflammation. *Frontiers in Neuroscience* **2017**, *11*.
(34) Aso, E.; Ferrer, I. CB2 Cannabinoid Receptor As Potential Target against Alzheimer's Disease. *Frontiers in Neuroscience* **2016**, *10*.
(35) Cassano, T.; Calcagnini, S.; Pace, L.; De Marco, F.; Romano, A.; Gaetani, S. Cannabinoid Receptor 2 Signaling in Neurodegenerative Disorders: From Pathogenesis to a Promising Therapeutic Target. *Frontiers in Neuroscience* **2017**, *11*.
(36) Mangiatordi, G. F.; Intranuovo, F.; Delre, P.; Abatematteo, F. S.; Abate, C.; Niso, M.; Creanza, T. M.; Ancona, N.; Stefanachi, A.; Contino, M. Cannabinoid Receptor Subtype 2 (CB2R) in a Multitarget Approach: Perspective of an Innovative Strategy in Cancer and Neurodegeneration. *J. Med. Chem.* **2020**, *63* (23), 14448–14469. https://doi.org/10.1021/acs.jmedchem.0c01357.
(37) Shoemaker, J. L.; Seely, K. A.; Reed, R. L.; Crow, J. P.; Prather, P. L. The CB2 Cannabinoid Agonist AM-1241 Prolongs Survival in a Transgenic Mouse Model of Amyotrophic Lateral Sclerosis When Initiated at Symptom Onset. *Journal of Neurochemistry* **2007**, *101* (1), 87–98. https://doi.org/10.1111/j.1471-4159.2006.04346.x.
(38) Croxford, J. L.; Miller, S. D. Immunoregulation of a Viral Model of Multiple Sclerosis Using the Synthetic Cannabinoid R(+)WIN55,212. *J Clin Invest* **2003**, *111* (8), 1231–1240. https://doi.org/10.1172/JCI17652.
(39) Calina, D.; Buga, A. M.; Mitroi, M.; Buha, A.; Caruntu, C.; Scheau, C.; Bouyahya, A.; El Omari, N.; El Menyiy, N.; Docea, A. O. The Treatment of Cognitive, Behavioural and Motor Impairments from Brain Injury and Neurodegenerative Diseases through Cannabinoid System Modulation—Evidence from In Vivo Studies. *Journal of Clinical Medicine* **2020**, *9* (8), 2395. https://doi.org/10.3390/jcm9082395.
(40) Guindon, J.; Hohmann, A. G. Cannabinoid CB2 Receptors: A Therapeutic Target for the Treatment of Inflammatory and Neuropathic Pain. *British Journal of Pharmacology* **2008**, *153* (2), 319–334. https://doi.org/10.1038/sj.bjp.0707531.
(41) Yao, B. B.; Hsieh, G. C.; Frost, J. M.; Fan, Y.; Garrison, T. R.; Daza, A. V.; Grayson, G. K.; Zhu, C. Z.; Pai, M.; Chandran, P.; Salyers, A. K.; Wensink, E. J.; Honore, P.; Sullivan, J. P.; Dart, M. J.; Meyer, M. D. In Vitro and in Vivo Characterization of A-796260: A Selective Cannabinoid CB2 Receptor Agonist Exhibiting Analgesic Activity in Rodent Pain Models. *British Journal of Pharmacology* **2008**, *153* (2), 390–401. https://doi.org/10.1038/sj.bjp.0707568.
(42) Cheng, Y.; Hitchcock, S. A. Targeting Cannabinoid Agonists for Inflammatory and Neuropathic Pain. *Expert Opinion on Investigational Drugs* **2007**, *16* (7), 951–965. https://doi.org/10.1517/13543784.16.7.951.
(43) Whiteside, G. T.; Lee, G. P.; Valenzano, K. J. The Role of the Cannabinoid CB2 Receptor in Pain Transmission and Therapeutic Potential of Small Molecule CB2 Receptor Agonists. *Current Medicinal Chemistry* **2007**, *14* (8), 917–936. https://doi.org/10.2174/092986707780363023.
(44) Lunn, C. A.; Fine, J. S.; Rojas-Triana, A.; Jackson, J. V.; Fan, X.; Kung, T. T.; Gonsiorek, W.; Schwarz, M. A.; Lavey, B.; Kozlowski, J. A.; Narula, S. K.; Lundell, D. J.; Hipkin, R. W.; Bober, L. A. A Novel Cannabinoid Peripheral Cannabinoid Receptor-Selective Inverse Agonist

Blocks Leukocyte Recruitment in Vivo. *J Pharmacol Exp Ther* **2006**, *316* (2), 780–788. https://doi.org/10.1124/jpet.105.093500.
(45) Xiang, W.; Shi, R.; Kang, X.; Zhang, X.; Chen, P.; Zhang, L.; Hou, A.; Wang, R.; Zhao, Y.; Zhao, K.; Liu, Y.; Ma, Y.; Luo, H.; Shang, S.; Zhang, J.; He, F.; Yu, S.; Gan, L.; Shi, C.; Li, Y.; Yang, W.; Liang, H.; Miao, H. Monoacylglycerol Lipase Regulates Cannabinoid Receptor 2-Dependent Macrophage Activation and Cancer Progression. *Nat Commun* **2018**, *9* (1), 2574. https://doi.org/10.1038/s41467-018-04999-8.
(46) Kisková, T.; Mungenast, F.; Suváková, M.; Jäger, W.; Thalhammer, T. Future Aspects for Cannabinoids in Breast Cancer Therapy. *International Journal of Molecular Sciences* **2019**, *20* (7), 1673. https://doi.org/10.3390/ijms20071673.
(47) Punzo, F.; Tortora, C.; Di Pinto, D.; Manzo, I.; Bellini, G.; Casale, F.; Rossi, F. Anti-Proliferative, pro-Apoptotic and Anti-Invasive Effect of EC/EV System in Human Osteosarcoma. *Oncotarget* **2017**, *8* (33), 54459–54471. https://doi.org/10.18632/oncotarget.17089.
(48) Punzo, F.; Manzo, I.; Tortora, C.; Pota, E.; Angelo, V. D.; Bellini, G.; Di Paola, A.; Verace, F.; Casale, F.; Rossi, F. Effects of CB2 and TRPV1 Receptors' Stimulation in Pediatric Acute T-Lymphoblastic Leukemia. *Oncotarget* **2018**, *9* (30), 21244–21258. https://doi.org/10.18632/oncotarget.25052.
(49) Velasco, G.; Sánchez, C.; Guzmán, M. Towards the Use of Cannabinoids as Antitumour Agents. *Nat Rev Cancer* **2012**, *12* (6), 436–444. https://doi.org/10.1038/nrc3247.
(50) Blázquez, C.; Carracedo, A.; Barrado, L.; Jose Real, P.; Luis Fernández-Luna, J.; Velasco, G.; Malumbres, M.; Guzmán, M.; Blázquez, C.; Carracedo, A. Cannabinoid Receptors as Novel Targets for the Treatment of Melanoma. *The FASEB journal* **2006**, *20* (14), 2633–2635.
(51) Steffens, S.; Veillard, N. R.; Arnaud, C.; Pelli, G.; Burger, F.; Staub, C.; Zimmer, A.; Frossard, J.-L.; Mach, F. Low Dose Oral Cannabinoid Therapy Reduces Progression of Atherosclerosis in Mice. *Nature* **2005**, *434* (7034), 782–786. https://doi.org/10.1038/nature03389.
(52) Lotersztajn, S.; Teixeira-Clerc, F.; Julien, B.; Deveaux, V.; Ichigotani, Y.; Manin, S.; Tran-Van-Nhieu, J.; Karsak, M.; Zimmer, A.; Mallat, A. CB2 Receptors as New Therapeutic Targets for Liver Diseases. *British Journal of Pharmacology* **2008**, *153* (2), 286–289. https://doi.org/10.1038/sj.bjp.0707511.
(53) Batkai, S.; Osei-Hyiaman, D.; Pan, H.; El-Assal, O.; Rajesh, M.; Mukhopadhyay, P.; Hong, F.; Harvey-White, J.; Jafri, A.; Haskó, G.; Huffman, J. W.; Gao, B.; Kunos, G.; Pacher, P. Cannabinoid-2 Receptor Mediates Protection against Hepatic Ischemia/Reperfusion Injury. *The FASEB Journal* **2007**, *21* (8), 1788–1800. https://doi.org/10.1096/fj.06-7451com.
(54) Pasquini, S.; Ligresti, A.; Mugnaini, C.; Semeraro, T.; Cicione, L.; De Rosa, M.; Guida, F.; Luongo, L.; De Chiaro, M.; Cascio, M. G.; Bolognini, D.; Marini, P.; Pertwee, R.; Maione, S.; Marzo, V. D.; Corelli, F. Investigations on the 4-Quinolone-3-Carboxylic Acid Motif. 3. Synthesis, Structure−Affinity Relationships, and Pharmacological Characterization of 6-Substituted 4-Quinolone-3-Carboxamides as Highly Selective Cannabinoid-2 Receptor Ligands. *J. Med. Chem.* **2010**, *53* (16), 5915–5928. https://doi.org/10.1021/jm100123x.
(55) Scheau, C.; Caruntu, C.; Badarau, I. A.; Scheau, A.-E.; Docea, A. O.; Calina, D.; Caruntu, A. Cannabinoids and Inflammations of the Gut-Lung-Skin Barrier. *Journal of Personalized Medicine* **2021**, *11* (6), 494. https://doi.org/10.3390/jpm11060494.
(56) Klein, T. W. Cannabinoid-Based Drugs as Anti-Inflammatory Therapeutics. *Nat Rev Immunol* **2005**, *5* (5), 400–411. https://doi.org/10.1038/nri1602.
(57) Hernández-Cervantes, R.; Méndez-Díaz, M.; Prospéro-García, Ó.; Morales-Montor, J. Immunoregulatory Role of Cannabinoids during Infectious Disease. *NIM* **2017**, *24* (4–5), 183–199. https://doi.org/10.1159/000481824.
(58) Sacerdote, P.; Massi, P.; Panerai, A. E.; Parolaro, D. In Vivo and in Vitro Treatment with the Synthetic Cannabinoid CP55,940 Decreases the in Vitro Migration of Macrophages in the Rat: Involvement of Both CB1 and CB2 Receptors. *Journal of Neuroimmunology* **2000**, *109* (2), 155–163. https://doi.org/10.1016/S0165-5728(00)00307-6.

(59) Costantino, C. M.; Gupta, A.; Yewdall, A. W.; Dale, B. M.; Devi, L. A.; Chen, B. K. Cannabinoid Receptor 2-Mediated Attenuation of CXCR4-Tropic HIV Infection in Primary CD4+ T Cells. *PLOS ONE* **2012**, *7* (3), e33961. https://doi.org/10.1371/journal.pone.0033961.
(60) Costiniuk, C. T.; Jenabian, M.-A. Cannabinoids and Inflammation: Implications for People Living with HIV. *AIDS* **2019**, *33* (15), 2273–2288. https://doi.org/10.1097/QAD.0000000000002345.
(61) Rock, R. B.; Gekker, G.; Hu, S.; Sheng, W. S.; Cabral, G. A.; Martin, B. R.; Peterson, P. K. WIN55,212-2-Mediated Inhibition of HIV-1 Expression in Microglial Cells: Involvement of Cannabinoid Receptors. *Jrnl Neuroimmune Pharm* **2007**, *2* (2), 178–183. https://doi.org/10.1007/s11481-006-9040-4.
(62) Rossi, F.; Tortora, C.; Argenziano, M.; Di Paola, A.; Punzo, F. Cannabinoid Receptor Type 2: A Possible Target in SARS-CoV-2 (CoV-19) Infection? *International Journal of Molecular Sciences* **2020**, *21* (11), 3809. https://doi.org/10.3390/ijms21113809.
(63) Savinainen, J. R.; Kokkola, T.; Salo, O. M. H.; Poso, A.; Järvinen, T.; Laitinen, J. T. Identification of WIN55212-3 as a Competitive Neutral Antagonist of the Human Cannabinoid CB2 Receptor. *British Journal of Pharmacology* **2005**, *145* (5), 636–645. https://doi.org/10.1038/sj.bjp.0706230.
(64) Zhou, L.; Zhou, S.; Yang, P.; Tian, Y.; Feng, Z.; Xie, X.-Q.; Liu, Y. Targeted Inhibition of the Type 2 Cannabinoid Receptor Is a Novel Approach to Reduce Renal Fibrosis. *Kidney International* **2018**, *94* (4), 756–772. https://doi.org/10.1016/j.kint.2018.05.023.
(65) Xiang, W.; Shi, R.; Kang, X.; Zhang, X.; Chen, P.; Zhang, L.; Hou, A.; Wang, R.; Zhao, Y.; Zhao, K.; Liu, Y.; Ma, Y.; Luo, H.; Shang, S.; Zhang, J.; He, F.; Yu, S.; Gan, L.; Shi, C.; Li, Y.; Yang, W.; Liang, H.; Miao, H. Monoacylglycerol Lipase Regulates Cannabinoid Receptor 2-Dependent Macrophage Activation and Cancer Progression. *Nat Commun* **2018**, *9* (1), 2574. https://doi.org/10.1038/s41467-018-04999-8.
(66) Deveaux, V.; Cadoudal, T.; Ichigotani, Y.; Teixeira-Clerc, F.; Louvet, A.; Manin, S.; Nhieu, J. T.-V.; Belot, M. P.; Zimmer, A.; Even, P.; Cani, P. D.; Knauf, C.; Burcelin, R.; Bertola, A.; Le Marchand-Brustel, Y.; Gual, P.; Mallat, A.; Lotersztajn, S. Cannabinoid CB2 Receptor Potentiates Obesity-Associated Inflammation, Insulin Resistance and Hepatic Steatosis. *PLoS One* **2009**, *4* (6), e5844. https://doi.org/10.1371/journal.pone.0005844.
(67) Fulo, H. F.; Shoeib, A.; Cabanlong, C. V.; Williams, A. H.; Zhan, C.-G.; Prather, P. L.; Dudley, G. B. Synthesis, Molecular Pharmacology, and Structure–Activity Relationships of 3-(Indanoyl)Indoles as Selective Cannabinoid Type 2 Receptor Antagonists. *J. Med. Chem.* **2021**, *64* (9), 6381–6396. https://doi.org/10.1021/acs.jmedchem.1c00442.
(68) Wang, M.; Hou, S.; Liu, Y.; Li, D.; Lin, J. Identification of Novel Antagonists Targeting Cannabinoid Receptor 2 Using a Multi-Step Virtual Screening Strategy. *Molecules* **2021**, *26* (21), 6679. https://doi.org/10.3390/molecules26216679.
(69) Pertwee, R. G. The Central Neuropharmcology of Psychotropic Cannabinoids. *Pharmacology & Therapeutics* **1988**, *36* (2), 189–261. https://doi.org/10.1016/0163-7258(88)90106-4.
(70) Debruyne, D.; Le Boisselier, R. Emerging Drugs of Abuse: Current Perspectives on Synthetic Cannabinoids. *Subst Abuse Rehabil* **2015**, *6*, 113–129. https://doi.org/10.2147/SAR.S73586.
(71) Li, X.; Hua, T.; Vemuri, K.; Ho, J.-H.; Wu, Y.; Wu, L.; Popov, P.; Benchama, O.; Zvonok, N.; Locke, K.; Qu, L.; Han, G. W.; Iyer, M. R.; Cinar, R.; Coffey, N. J.; Wang, J.; Wu, M.; Katritch, V.; Zhao, S.; Kunos, G.; Bohn, L. M.; Makriyannis, A.; Stevens, R. C.; Liu, Z.-J. Crystal Structure of the Human Cannabinoid Receptor CB2. *Cell* **2019**, *176* (3), 459-467.e13. https://doi.org/10.1016/j.cell.2018.12.011.
(72) Rinaldi-Carmona, M.; Barth, F.; Héaulme, M.; Shire, D.; Calandra, B.; Congy, C.; Martinez, S.; Maruani, J.; Néliat, G.; Caput, D.; Ferrara, P.; Soubrié, P.; Brelière, J. C.; Le Fur, G.

SR141716A, a Potent and Selective Antagonist of the Brain Cannabinoid Receptor. *FEBS Letters* **1994**, *350* (2), 240–244. https://doi.org/10.1016/0014-5793(94)00773-X.
(73) Longworth, M.; Connor, M.; Banister, S. D.; Kassiou, M. Synthesis and Pharmacological Profiling of the Metabolites of Synthetic Cannabinoid Drugs APICA, STS-135, ADB-PINACA, and 5F-ADB-PINACA. *ACS Chem. Neurosci.* **2017**, *8* (8), 1673–1680. https://doi.org/10.1021/acschemneuro.7b00116.
(74) Aly, M. W.; Ludwig, F.-A.; Deuther-Conrad, W.; Brust, P.; Abadi, A. H.; Moldovan, R.-P.; Osman, N. A. Development of Fluorinated and Methoxylated Benzothiazole Derivatives as Highly Potent and Selective Cannabinoid CB2 Receptor Ligands. *Bioorg Chem* **2021**, *114*, 105191. https://doi.org/10.1016/j.bioorg.2021.105191.
(75) Faúndez-Parraguez, M.; Alarcón-Miranda, C.; Cho, Y. H.; Pessoa-Mahana, H.; Gallardo-Garrido, C.; Chung, H.; Faúndez, M.; Pessoa-Mahana, D. New Pyridone-Based Derivatives as Cannabinoid Receptor Type 2 Agonists. *International Journal of Molecular Sciences* **2021**, *22* (20), 11212. https://doi.org/10.3390/ijms222011212.
(76) Stern, E.; Muccioli, G. G.; Bosier, B.; Hamtiaux, L.; Millet, R.; Poupaert, J. H.; Hénichart, J.-P.; Depreux, P.; Goossens, J.-F.; Lambert, D. M. Pharmacomodulations around the 4-Oxo-1,4-Dihydroquinoline-3-Carboxamides, a Class of Potent CB2-Selective Cannabinoid Receptor Ligands: Consequences in Receptor Affinity and Functionality. *J. Med. Chem.* **2007**, *50* (22), 5471–5484. https://doi.org/10.1021/jm070387h.
(77) Uchiyama, N.; Kawamura, M.; Kikura-Hanajiri, R.; Goda, Y. Identification of Two New-Type Synthetic Cannabinoids, N-(1-Adamantyl)-1-Pentyl-1H-Indole-3-Carboxamide (APICA) and N-(1-Adamantyl)-1-Pentyl-1H-Indazole-3-Carboxamide (APINACA), and Detection of Five Synthetic Cannabinoids, AM-1220, AM-2233, AM-1241, CB-13 (CRA-13), and AM-1248, as Designer Drugs in Illegal Products. *Forensic Toxicol* **2012**, *30* (2), 114–125. https://doi.org/10.1007/s11419-012-0136-7.
(78) Ragusa, G.; Gómez-Cañas, M.; Morales, P.; Rodríguez-Cueto, C.; Pazos, M. R.; Asproni, B.; Cichero, E.; Fossa, P.; Pinna, G. A.; Jagerovic, N.; Fernández-Ruiz, J.; Murineddu, G. New Pyridazinone-4-Carboxamides as New Cannabinoid Receptor Type-2 Inverse Agonists: Synthesis, Pharmacological Data and Molecular Docking. *European Journal of Medicinal Chemistry* **2017**, *127*, 398–412. https://doi.org/10.1016/j.ejmech.2017.01.002.
(79) Moldovan, R.-P.; Hausmann, K.; Deuther-Conrad, W.; Brust, P. Development of Highly Affine and Selective Fluorinated Cannabinoid Type 2 Receptor Ligands. *ACS Med. Chem. Lett.* **2017**, *8* (5), 566–571. https://doi.org/10.1021/acsmedchemlett.7b00129.
(80) Creanza, T. M.; Lamanna, G.; Delre, P.; Contino, M.; Corriero, N.; Saviano, M.; Mangiatordi, G. F.; Ancona, N. DeLA-Drug: A Deep Learning Algorithm for Automated Design of Druglike Analogues. *J. Chem. Inf. Model.* **2022**, *62* (6), 1411–1424. https://doi.org/10.1021/acs.jcim.2c00205.
(81) Xing, C.; Zhuang, Y.; Xu, T.-H.; Feng, Z.; Zhou, X. E.; Chen, M.; Wang, L.; Meng, X.; Xue, Y.; Wang, J.; Liu, H.; McGuire, T. F.; Zhao, G.; Melcher, K.; Zhang, C.; Xu, H. E.; Xie, X.-Q. Cryo-EM Structure of the Human Cannabinoid Receptor CB2-Gi Signaling Complex. *Cell* **2020**, *180* (4), 645-654.e13. https://doi.org/10.1016/j.cell.2020.01.007.
(82) Manera, C.; Benetti, V.; Castelli, M. P.; Cavallini, T.; Lazzarotti, S.; Pibiri, F.; Saccomanni, G.; Tuccinardi, T.; Vannacci, A.; Martinelli, A.; Ferrarini, P. L. Design, Synthesis, and Biological Evaluation of New 1,8-Naphthyridin-4(1H)-on-3-Carboxamide and Quinolin-4(1H)-on-3-Carboxamide Derivatives as CB2 Selective Agonists. *J Med Chem* **2006**, *49* (20), 5947–5957. https://doi.org/10.1021/jm0603466.
(83) Iwamura, H.; Suzuki, H.; Ueda, Y.; Kaya, T.; Inaba, T. In Vitro and in Vivo Pharmacological Characterization of JTE-907, a Novel Selective Ligand for Cannabinoid CB2 Receptor. *J Pharmacol Exp Ther* **2001**, *296* (2), 420–425.

(84) Dreskin, S. C.; Thomas, G. W.; Dale, S. N.; Heasley, L. E. Isoforms of Jun Kinase Are Differentially Expressed and Activated in Human Monocyte/Macrophage (THP-1) Cells. *J Immunol* **2001**, *166* (9), 5646–5653. https://doi.org/10.4049/jimmunol.166.9.5646.
(85) Mugnaini, C.; Kostrzewa, M.; Bryk, M.; Mahmoud, A. M.; Brizzi, A.; Lamponi, S.; Giorgi, G.; Ferlenghi, F.; Vacondio, F.; Maccioni, P.; Colombo, G.; Mor, M.; Starowicz, K.; Di Marzo, V.; Ligresti, A.; Corelli, F. Correction to Design, Synthesis, and Physicochemical and Pharmacological Profiling of 7-Hydroxy-5-Oxopyrazolo[4,3-b]Pyridine-6-Carboxamide Derivatives with Antiosteoarthritic Activity In Vivo. *J Med Chem* **2020**, *63* (19), 11303. https://doi.org/10.1021/acs.jmedchem.0c01567.
(86) Protein Preparation Wizard, LLC, New York, NY, 2021.
(87) Lu, C.; Wu, C.; Ghoreishi, D.; Chen, W.; Wang, L.; Damm, W.; Ross, G. A.; Dahlgren, M. K.; Russell, E.; Von Bargen, C. D.; Abel, R.; Friesner, R. A.; Harder, E. D. OPLS4: Improving Force Field Accuracy on Challenging Regimes of Chemical Space. *J. Chem. Theory Comput.* **2021**, *17* (7), 4291–4300. https://doi.org/10.1021/acs.jctc.1c00302.
(88) LigPrep, Schrödinger, LLC, New York, NY, 2021.
(89) Kaminski, G. A.; Friesner, R. A.; Tirado-Rives, J.; Jorgensen, W. L. Evaluation and Reparametrization of the OPLS-AA Force Field for Proteins via Comparison with Accurate Quantum Chemical Calculations on Peptides. *J. Phys. Chem. B* **2001**, *105* (28), 6474–6487. https://doi.org/10.1021/jp003919d.
(90) Delre, P.; Caporuscio, F.; Saviano, M.; Mangiatordi, G. F. Repurposing Known Drugs as Covalent and Non-Covalent Inhibitors of the SARS-CoV-2 Papain-Like Protease. *Frontiers in Chemistry* **2020**, *8*.
(91) Genheden, S.; Ryde, U. The MM/PBSA and MM/GBSA Methods to Estimate Ligand-Binding Affinities. *Expert Opin Drug Discov* **2015**, *10* (5), 449–461. https://doi.org/10.1517/17460441.2015.1032936.

Graphical Abstract.

***N*-ADAMANTYL-ANTHRANIL AMIDE DERIVATIVES: NEW SELECTIVE LIGANDS FOR THE CANNABINOID RECEPTOR SUBTYPE 2 (CB2R)**